An efficient full-wave solver for eddy currents

Johan Helsing[a,1], Anders Karlsson[b], Andreas Rosén[c,*]

[a]*Centre for Mathematical Sciences, Lund University, Box 118, 221 00, Lund, Sweden*
[b]*Electrical and Information Technology, Lund University, Box 118, 221 00, Lund, Sweden*
[c]*Mathematical Sciences, Chalmers University of Technology and the University of Gothenburg, 412 96, Gothenburg, Sweden*

Abstract

An integral equation reformulation of the Maxwell transmission problem is presented. The reformulation uses techniques such as tuning of free parameters and augmentation of close-to-rank-deficient operators. It is designed for the eddy current regime and works both for surfaces of genus 0 and 1. Well-conditioned systems and field representations are obtained despite the Maxwell transmission problem being ill-conditioned for genus 1 surfaces due to the presence of Neumann eigenfields. Furthermore, it is shown that these eigenfields, for ordinary conductors in the eddy current regime, are different from the classical Neumann eigenfields for superconductors. Numerical examples, based on the reformulation, give an unprecedented 13-digit accuracy both for transmitted and scattered fields.

Keywords: Maxwell transmission problem, Eddy current, Boundary integral equation, Neumann eigenfield, Low-frequency breakdown
2010 MSC: 15A66, 35Q61, 45E05, 78M99

1. Introduction

This work concerns the Maxwell transmission problem (MTP), which is the problem of computing the electromagnetic wave transmitted through and scattered from a bounded object $\Omega_+ \subset \mathbf{R}^3$, given an incident time-harmonic electromagnetic wave in the exterior region $\Omega_- = \mathbf{R}^3 \setminus \overline{\Omega}_+$. Consider Ω_+ with boundary surface Γ, generalized diameter $L = \sup\{|x - y| \; ; \; x, y \in \Omega_+\}$ and Ω_- being vacuum. The corresponding wavenumbers are

$$k_+ = \omega\sqrt{(\epsilon_0\epsilon_r + i\sigma/\omega)\mu_0}\,, \tag{1}$$

$$k_- = \omega\sqrt{\epsilon_0\mu_0}\,, \tag{2}$$

where $\omega, \epsilon_0, \mu_0, \epsilon_r, \sigma$ denote frequency, permittivity and permeability of vacuum, and relative permittivity and conductivity of Ω_+. In terms of the wavenumbers, the conductivity is $\sigma = \mathrm{Re}(k_+^2/(i\eta_0 k_-))$ and the skin depth equals $1/\mathrm{Im}(k_+)$. Since magnetic materials often have nonlinear properties and exhibit hysteresis we restrict ourselves to non-magnetic materials, for which the linear MTP (7) below is an accurate physical model.

As $\sigma \to \infty$ for fixed $\omega > 0$, the object Ω_+ approaches a perfect electric conductor (PEC) with zero internal fields and with the electric field normal and the magnetic field tangential to Γ. The PEC boundary condition, that the electric field is normal to Γ, is only proper if the skin depth is much smaller than the diameter of the object. This is why the PEC boundary condition cannot be applied to metals at low frequencies. On the other hand it applies, with good accuracy, to a superconductor for frequencies ranging from zero up to very high values. The reason is that a superconductor is also a perfect diamagnet. Therefore we refer to the limit $\sigma \to \infty$ for the MTP as the *superconducting limit*, despite restricting ourselves to non-magnetic materials.
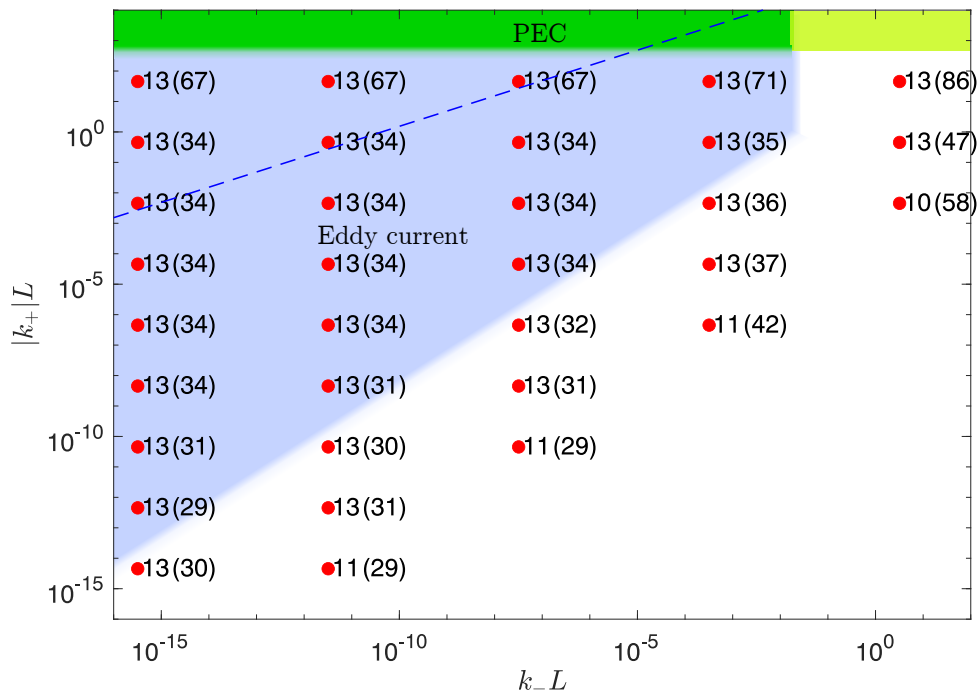
---

*Corresponding author

Figure 1: Performance of Dirac (B-aug1) on the "starfish torus" (71) with incident partial waves (44) and $\arg(k_+) = \pi/4$. The expression $Y(X)$ at red points $(k_- L, |k_+|L)$ says that GMRES needs X iterations and that Y-digit accuracy (74), or better, is achieved in each of the fields $\{E^+, E^-, H^+, H^-\}$ at all 90,000 field points in the computational domain. The PEC regime is in dark green and light green. The eddy current regime is in blue and dark green (vacuum in Ω_-). The dashed line is the upper limit of realizable $|k_+|L$ for $L = 1$ m (silver in Ω_+, vacuum in Ω_-). Red points outside the eddy current regime, with $\arg(k_+) = \pi/4$, can be realized if Ω_- is a dielectric.

In scattering theory, the regime $k_- L \ll 1$ is referred to as the Rayleigh regime. Here the scattered far fields are accurately determined by the induced electric and magnetic dipole moments in Ω_+, an approximation widely used in optics and microwave theory [21, Sec. 10.1] and with application in radar, lidar, and radio communication [29, 20, 28]. The scattered near fields from sub-wavelength objects are important in non-destructive testing, where they serve as input data to solvers that extract information about the objects' interior [13, 8]. The design of integrated circuits often requires the determination of inductances, capacitances, and resistances of sub-wavelength components based on both transmitted and scattered fields [33].

When $\sigma/\omega \gg \epsilon_0 \epsilon_r$, then $\arg(k_+) \approx \pi/4$ in (1) and

$$|k_+|L \approx \sqrt{\eta_0 \sigma L} \sqrt{k_- L}, \tag{3}$$

where also $|k_+|L \gg k_- L$. We refer to σL as the *scaled conductivity* of Ω_+. Here $\eta_0 \sigma L$ and $k_- L$ are dimensionless, and $\eta_0 = \sqrt{\mu_0/\epsilon_0} \approx 377$ Ohm is the wave impedance of vacuum. The pair of wavenumbers (k_-, k_+) is said to be in the *eddy current regime* if $L \ll 1/k_-$ and $|k_+| \gg k_-$. The eddy current regime is in blue and dark green in Figure 1. There is an upper limit on conductivity $\sigma \lesssim 6 \cdot 10^7$ S/m in ordinary conductors, that is, non-superconducting materials. Thus $|k_+|L \lesssim C\sqrt{k_- L}$, where $C \approx 1.5 \cdot 10^5 \sqrt{L}$ with L measured in meters, is the physical part of the eddy current regime for objects of given size L. When $L = 1$ m this limit is the dashed line in Figure 1. The low-frequency asymptote for any ordinary conductor with $\sigma > 0$ and $L = 1$ m, is a line parallel to, and below, this dashed line. The dark green and light green areas in Figure 1 is the regime where the PEC boundary condition is applicable with a reasonably small relative error. To stay in this area when $\omega \to 0$, it is necessary that $\sigma \to \infty$. It is seen that for $L = 1$ m and $k_- L < 10^{-5}$ the PEC approximation is invalid for ordinary conductors, but it holds for superconductors. This is so since the surface resistance of a superconductor is low enough to be considered to be zero in the entire eddy current regime, see [16], and zero surface resistance implies the PEC boundary condition on Γ.

We refer to solvers based on boundary integral equations (BIEs) that model the full MTP

as *full-wave solvers*, in contrast to solvers which build on an approximation to the MTP. When $|k_+|L \ll 1$, a standard approximation is to determine the dipole moments by solving Laplace's equation, and for $|k_+|L \gg 1$ the standard approximation is to use the PEC boundary condition. Between these two extremes it is necessary to solve the MTP without approximations. The full-wave solvers for the MTP in the eddy current regime that we have found in the literature are [27, 33, 4]. Rucker et al. [27] give an overview of full-wave solvers, which give at best a relative error of 1% in scattering situations comparable to our Figure 3. Zhu et al. [33] describe a full-wave solver used for an open source program FastImp. Chhim et al. [4] present a full-wave solver based on the PMCHWT BIE. We lack data to judge the accuracy of the BIEs in [33] and [4]. The analysis in [4] appears to be limited to $\omega \to 0$ for fixed σ, leaving a possible gap to the green PEC regime in Figure 1. Also, numerical evaluation of the field representations is missing in [4], cf. Section 8.5. Other BIEs rather solve the quasi-static approximation of the MTP obtained by neglecting the dispacement current in Ampère's law, which limits their validity. For justifications of such eddy current models, see [1, 25, 3]. As these rather sparse results in the literature indicate, it is indeed a challenging problem to design BIEs for the MTP in the eddy current regime. As we discuss below, reasons for this is that the fields may differ much in size and for Γ of non-zero genus the MTP itself is actually ill-posed in the eddy current regime as $k_- \to 0$. By the limit being in the eddy current regime, we mean that $|k_+|/k_- \to \infty$. More precisely, in such limits there is an incident field for which some of the transmitted and scattered fields differ drastically from their generic magnitude. We refer to Sections 5, 8.3 and 8.4 for details. See Hiptmair [19] for more background on eddy current computations.

For our numerical method to be efficient when $\mathrm{Im}\,(k_+)$ is large, we always assume that $|k_+|L \lesssim 50$, so our standing assumption in numerical evaluations is that

$$0 < k_- L \ll |k_+|L \lesssim 50. \tag{4}$$

In this paper, we achieve BIEs that compute all the fields to a minimum of 13 accurate digits in the entire regime (4), for Γ of genus 0 as well as genus 1. See Figure 8 in Section 8.6 for genus 0 and Figure 1 for genus 1. Our BIEs appear to be the only known full-wave solvers for the MTP that compute all fields accurately and fast in all of (4). We point out that although $\arg(k_-) = 0$ and $\arg(k_+) = \pi/4$ in all our numerical examples, there is no approximation of the full MTP (7) involved, and a known permittivity can be included in k_+.

The Dirac BIE from [18, 17] is the starting point for the present work and from now on referred to as Dirac (A). This BIE is based on the embedding of Maxwell's equations into an elliptic Dirac equation and a Cauchy integral representation for the fields (Eq. (28) below). Schematically, given the incident wave g on Γ, we have

$$h \mapsto (F^+, F^-) \mapsto g, \tag{5}$$

and solve the Dirac BIE for the density h on Γ, from which the ansatz/Cauchy representation yields the transmitted electric and magnetic fields $F^+ = (E^+, H^+)$ in Ω_+ and the scattered fields $F^- = (E^-, H^-)$ in Ω_-. The Dirac BIE is a size 8×8 block system using 50, not all distinct, integral operators of double and single layer type, which can be used on any Lipschitz regular boundary Γ. It has 12 free parameters, as recalled in (24) below, and these can be chosen to avoid false eigenwavenumbers for all passive materials. As for low-frequency breakdown, the only regimes found in [18, 17] where the Dirac (A) exhibits false eigenwavenumbers is when $k_\pm \to 0$ at the same time as $\hat{k} = k_+/k_- \to \infty$ or $\hat{k} \to 0$. (We refer to [17, Sec. 3] for a discussion about the notions of eigenwavenumbers and low-frequency breakdown. See also Section 4 for the notions of dense-mesh breakdown and topological low-frequency breakdown.) This corresponds to the false eigenwavenumber at $x = -1$ in [17, Fig. 9(b)], and it should be noted that this single peak contains the whole eddy current regime shown in Figure 1. (The reverse eddy current regime corresponding to $x = +1$, where the roles of $\Omega_\pm$ have been swapped, is less important in applications, and we omit the details.)

The design of all Dirac BIEs starts by *tuning*, that is, carefully assigning values to the free parameters, to avoid false eigenwavenumbers and optimize numerical performance. The main result of this paper consists of two new parameter choices for Dirac BIEs in the eddy current regime, referred to as Dirac (A∞) and Dirac (B), which, at a low cost, enable us to simultaneously compute the four fields $\{E^+, E^-, H^+, H^-\}$ to almost full machine precision. A key problem in the

3

eddy current regime is that the fields $\{E^+, E^-, H^+, H^-\}$ may differ much in size, and tuning the parameters to account for this becomes a non-trivial matter. In particular, the transmitted electric field E^+ is typically much smaller than the other fields. It is nevertheless important to compute also E^+ with a small relative error, since the measurable eddy current $J = \sigma E^+$ will have the same relative error.

An important take-home message from the present paper is that in order to stably solve the MTP through (5), it is necessary both (a) to have a well-conditioned BIE for computing the density h from the boundary datum g, and (b) to have a well-conditioned representation of the fields, for computing the fields $F^\pm$ from the density h. For Dirac (A∞), it is in general (b) that is problematic since its field evaluation allows for large fields, see (50), and this sometimes leads to cancellation and loss of accuracy for small fields like E^+. Dirac (B) is adapted to the small size of E^+, see (54). It is then rather (a) which is challenging, but we still obtain a well-conditioned system. To eliminate null densities h we use *augmentation*, that is we suitably add a finite-rank matrix to the system to be solved, without changing the physical solutions. We explain in Sections 3 and 4 our general process for designing Dirac BIEs. The augmentation techniques explained in Section 4 are of independent interest beyond the MTP. After such augmentations, which for our BIEs are needed only as $k_- \to 0$, we obtain BIEs referred to as (A∞-aug) and (B-aug0/1) for the MTP. Our augmentations build on a careful analysis of null spaces and ranges of the quasi-static limit operators, given in the Appendix. In absense of such detailed knowledge one could try random augmentations as in [30]. However, most of our operators require a careful choice of augmentation or else well-conditioning and accuracy will be lost.

Turning to objects Ω_+ with non-zero genus, an additional difficulty at high scaled conductivities is that Neumann eigenfields, similar to those in PEC scattering [7, 9], appear also in the MTP in the eddy current regime as $k_- \to 0$. More surprisingly, such Neumann eigenfields are present at low frequencies even for finite non-zero scaled conductivities, although the terminology "eigenfield" may not be appropriate to describe this phenomenon. The same Neumann eigenfield appears in the low-frequency limit for all ordinary conductors, regardless of the value of σ. We have not found this Neumann eigenfield for ordinary conductors in the literature. In particular it is not related to the notion of k-Neumann fields from [23, 10, 11], since it is a static field and the magnetic field is not tangential on the surface. However, when $\sigma \to \infty$ as $\omega \to 0$, our Neumann eigenfield approaches the classical static PEC Neumann eigenfield. See (45) and numerical examples and discussion in Sections 8.3 and 8.4, where it is shown that there exists an incident field for which some of the transmitted and scattered fields differ drastically from their generic magnitude. This means that for Γ of non-zero genus, the MTP itself is ill-conditioned in the eddy current regime. We discuss the Neumann eigenfields in some detail in Section 5, and here only stress one important point: according to our discussion above, the physical eddy current eigenfields appearing in ordinary conductors are those shown in Figure 2(g,h,i). The Neumann eigenfields computed with the PEC boundary condition appear only in superconductors. See Figure 2(a,b,c).

At the end of the paper, we give in Section 9 a proof of the result, which we have not found in the literature, that the essential spectrum of the MTP coincides with that of the Neumann–Poincaré operator. This proof further illustrates the flexibility of the free Dirac parameters. We conclude the paper in Section 10 with some remarks on the usage of (A∞-aug) and (B-aug0/1).

2. The Maxwell and the two Helmholtz problems

We fix notation for the remainder of the paper. Let Ω_+ be a bounded, connected domain in $\mathbf{R}^3$ with Lipschitz regular boundary surface Γ and an unbounded, connected, exterior Ω_-. Let $L = \sup\{|x - y| \; ; \; x, y \in \Omega_+\}$ be the generalized diameter of Ω_+. Starting from Section 6, we use unit of length so that L is of order 1, which is convenient in numerical computations. The outward unit normal on Γ is ν, surface measure is $d\Gamma$, and $\{\nu, \tau, \theta\}$ denotes a positive ON-frame on Γ. (Singularities of the frame on a null set does not present a problem.) In $\mathbf{R}^3$, $\{\boldsymbol{\rho}, \boldsymbol{\theta}, \boldsymbol{z}\}$ denotes the standard cylindrical ON-frame. We consider time-harmonic fields with time dependence $e^{-i\omega t}$, and angular frequency $\omega > 0$. The domains $\Omega_\pm$ are homogeneous with material properties described by wavenumbers $k_\pm$, and we write

$$\hat{k} = k_+/k_-. \tag{6}$$

All our numerical examples use $\arg(k_-) = 0$ and $\arg(k_+) = \pi/4$, but our BIEs (A∞) and (B-aug0/1) apply to more general wavenumbers $\mathrm{Im}\,(k_\pm) \geq 0$ satisfying (4).

We consider Maxwell transmission problems MTP(k_-, k_+, α)

$$\begin{cases} \nu \times E^+ = \nu \times (E^0 + E^-), & x \in \Gamma, \\ \nu \times H^+ = (\hat{k}^2/\alpha)\nu \times (H^0 + H^-), & x \in \Gamma, \\ \nabla \times E^+ = ik_+(\hat{k}^{-1}H^+), \quad \nabla \times (\hat{k}^{-1}H^+) = -ik_+ E^+, & x \in \Omega_+, \\ \nabla \times E^- = ik_- H^-, \quad \nabla \times H^- = -ik_- E^-, & x \in \Omega_-, \\ x/|x| \times E^- - H^- = o(|x|^{-1}e^{\mathrm{Im}\,(k_-)|x|}), & x \to \infty, \\ x/|x| \times H^- - E^- = o(|x|^{-1}e^{\mathrm{Im}\,(k_-)|x|}), & x \to \infty, \end{cases} \tag{7}$$

where E^0 and H^0 are the incident fields from sources in Ω_-, and we want to solve for $E^\pm$ and $H^\pm$. In particular

$$\int_\Gamma \nu \cdot E^- \, d\Gamma = 0 \tag{8}$$

holds by the jump relations and the divergence theorem. For a discussion of the L_2 topology considered for the fields and the corresponding trace space, we refer to [18, Sec. 5]. The physical Maxwell transmission problem that we aim to solve is MTP(k_-, k_+)= MTP$(k_-, k_+, \hat{k}^2)$, with $\alpha = \hat{k}^2$, where the tangential parts of both the electric and magnetic fields are continuous across Γ. However, we also use auxiliary MTPs with other values of the parameter α.

Remark 1. The $k_\pm$ are related to the total permittivities $\epsilon_\pm$ and permeabilities $\mu_\pm$ by $k_\pm = \omega\sqrt{\epsilon_\pm \mu_\pm}$ in $\Omega_\pm$ respectively. We follow the convention from [17] where in all $\mathbf{R}^3$, the H field is the magnetic field rescaled by the wave impedance $\sqrt{\mu_-/\epsilon_-}$. The field $\hat{k}^{-1}H^+$, appearing in (7), is the magnetic field rescaled by the wave impedance $\sqrt{\mu_+/\epsilon_+}$ in Ω_+. This field is natural when formulating Maxwell's equations as a Dirac equation, and was denoted B^+ in [18].

Besides MTPs, we also consider auxiliary Helmholtz transmission problems HTP(k_-, k_+, β)

$$\begin{cases} u^+ = u^0 + u^-, & x \in \Gamma, \\ \partial_\nu u^+ = \beta \partial_\nu (u^0 + u^-), & x \in \Gamma, \\ \Delta U^+ + k_+^2 U^+ = 0, & x \in \Omega_+, \\ \Delta U^- + k_-^2 U^- = 0, & x \in \Omega_-, \\ \partial_{x/|x|}U^- - ik_- U^- = o(|x|^{-1}e^{\mathrm{Im}\,(k_-)|x|}), & x \to \infty, \end{cases} \tag{9}$$

where u^0 is the trace of the incident wave U^0, and we want to solve for $U^\pm$. We use the elliptic Dirac type equation

$$\begin{bmatrix} 0 & \nabla\cdot & 0 & 0 \\ \nabla & 0 & -\nabla\times & 0 \\ 0 & \nabla\times & 0 & \nabla \\ 0 & 0 & \nabla\cdot & 0 \end{bmatrix} \begin{bmatrix} F_0 \\ F_1 \\ F_2 \\ F_3 \end{bmatrix} = ik \begin{bmatrix} F_0 \\ F_1 \\ F_2 \\ F_3 \end{bmatrix}, \tag{10}$$

for two scalar fields F_0 and F_3, and two vector fields F_1 and F_2, which embeds one Maxwell and two Helmholtz equations. Indeed, for $F_0 = F_3 = 0$, (10) amounts to Maxwell's equations for $F_1 = E^+$ and

$$F_2 = \hat{k}^{-1}H^+ \tag{11}$$

in Ω_+, and for $F_1 = E^-$ and $F_2 = H^-$ in Ω_-. Moreover, the Helmholtz equation for U amounts to (10) for $F_0 = ikU$, $F_1 = \nabla U$ and $F_2 = F_3 = 0$, as well as for $F_3 = ikU$, $F_2 = \nabla U$ and $F_0 = F_1 = 0$. A main point with the Dirac formalism is that it avoids divergence- and curl-free constraints, by complementing the divergence-free Maxwell vector fields with the Helmholtz gradient vector fields.

The Dirac transmission problem DTP$(k_-, k_+, \alpha, \beta, \gamma)$ which is fundamental in our formalism is

$$\begin{cases} F^+ = M(F^0 + F^-), & x \in \Gamma, \\ \mathbf{D}F^+ = ik_+ F^+, & x \in \Omega_+, \\ \mathbf{D}F^- = ik_- F^-, & x \in \Omega_-, \\ (x/|x| - 1)F^- = o(|x|^{-1}e^{\mathrm{Im}\,(k_-)|x|}), & x \to \infty. \end{cases} \tag{12}$$

5

The Dirac derivative $\mathbf{D}F$ is the left-hand side in (10), and replacing ∇ by the vector x in this matrix yields the Clifford product xF appearing in the Dirac radiation condition. (For a short explanation of the underlying multivector formalism we refer to [18, Sec. 3], and for the long explanation we refer to [26].) On Γ, we write Dirac fields F as

$$F = \begin{bmatrix} F_0 & \nu \cdot F_2 & \boldsymbol{F}_{2T} & F_3 & \nu \cdot F_1 & \boldsymbol{F}_{1T} \end{bmatrix}, \tag{13}$$

with tangential fields $\boldsymbol{F}_{jT} = (\tau \cdot F_j)\tau + (\theta \cdot F_j)\theta$, $j = 1, 2$. The jump matrix M is the diagonal matrix

$$M = \mathrm{diag} \begin{bmatrix} \hat{k}/(\alpha\beta) & 1/\hat{k} & \hat{\boldsymbol{k}}/\boldsymbol{\alpha} & 1/\gamma & 1/\alpha & \mathbf{1} \end{bmatrix}, \tag{14}$$

when acting on F in (13). This special structure of M ensures that the DTP decouples in a certain way into one MTP with parameter α and two HTPs with parameters β and γ. See [18, Prop. 8.4].

For a given wavenumber k, the Dirac equation $\mathbf{D}F = ikF$ comes with a Cauchy reproducing formula for F, similar to the classical one for analytic functions and $k = 0$. When acting on F, written as in (13), the singular Cauchy integral on Γ is

$$E_k = \begin{bmatrix} -K_k^{\nu'} & 0 & \boldsymbol{K}_{1,3:4} & 0 & S_k & \mathbf{0} \\ K_{2,1} & -K_k^{\nu} & \boldsymbol{K}_{2,3:4} & S_{2,5} & 0 & \boldsymbol{S}_{2,7:8} \\ \boldsymbol{K}_{3:4,1} & \boldsymbol{K}_{3:4,2} & -\boldsymbol{M}_k^* & \boldsymbol{S}_{3:4,5} & \mathbf{0} & \boldsymbol{S}_{3:4,7:8} \\ 0 & S_k & \mathbf{0} & -K_k^{\nu'} & 0 & \boldsymbol{K}_{5,7:8} \\ S_{6,1} & 0 & \boldsymbol{S}_{6,3:4} & K_{6,5} & -K_k^{\nu} & \boldsymbol{K}_{6,7:8} \\ \boldsymbol{S}_{7:8,1} & \mathbf{0} & \boldsymbol{S}_{7:8,3:4} & \boldsymbol{K}_{7:8,5} & \boldsymbol{K}_{7:8,6} & -\boldsymbol{M}_k^* \end{bmatrix}. \tag{15}$$

In this paper, we enumerate the scalar components of Dirac fields (13) by $1, \ldots, 8$, and use boldface vector notation for the tangential vectors parts 3:4 and 7:8. We denote the causal fundamental solution to the Helmholtz equation, normalized with a factor of -2, by

$$\Phi_k(x) = \frac{e^{ik|x|}}{2\pi|x|}. \tag{16}$$

The operators appearing along the diagonal are the acoustic double layer

$$K_k^{\nu'} f(x) = \mathrm{p.v.} \int_\Gamma \nabla \Phi_k(y - x) \cdot \nu(y) f(y) d\Gamma(y) \tag{17}$$

with real adjoint $-K_k^{\nu} f$, where $\nu(y)$ is replaced by $\nu(x)$, and the real adjoint $\boldsymbol{M}_k^*$ of the acoustic magnetic dipole operator

$$\boldsymbol{M}_k f(x) = \nu(x) \times \mathrm{p.v.} \int_\Gamma \nabla \Phi_k(y - x) \times f(y) d\Gamma(y). \tag{18}$$

Also appearing is the acoustic single layer

$$S_k f(x) = ik \int_\Gamma \Phi_k(y - x) f(y) d\Gamma(y), \tag{19}$$

with the scaling factor ik. The remaining operators K and S include various products of the frame vectors $\{\nu, \tau, \theta\}$ and are detailed in [17, Eq. (27)].

A fundamental algebraic property of E_k is that for each wavenumber $k \in \mathbf{C}$, we have $E_k^2 = I$. Using the associated Hardy projections

$$E_k^\pm = \tfrac{1}{2}(I \pm E_k), \tag{20}$$

we can express DTP$(k_-, k_+, \alpha, \beta, \gamma)$ compactly as

$$\begin{cases} F^+ = M(F^0 + F^-), \\ E_{k_+}^- F^+ = 0, \\ E_{k_-}^+ F^- = 0, \end{cases} \tag{21}$$

for $F^\pm$ and F^0 on Γ. The condition $E_{k_+}^- F^+ = 0$ is equivalent to F^+ belonging to the range of the projection operator $E_{k_+}^+$, that is, F^+ is the trace of a solution to $\mathbf{D}F^+ = ik_+ F^+$ in Ω^+. Similarly $E_{k_-}^+ F^- = 0$ encodes that F^- is the trace of an exterior Dirac solution with wavenumber k_-, which satisfies the Dirac radiation condition.

3. The Dirac integral equation

In [18], BIEs for $\mathrm{DTP}(k_-, k_+, \alpha, \beta, \gamma)$ were derived as follows. We make a field representation $F^+ = rE^+_{k_+}(M'P'h)$, $F^- = -E^-_{k_-}(P'h)$ and multiply the jump relation $F^+ = M(F^- + F^0)$ by P. In matrix notation, this amounts to the BIE

$$P \begin{bmatrix} E^+_{k_+} & -ME^-_{k_-} \end{bmatrix} \begin{bmatrix} r & 0 \\ 0 & 1 \end{bmatrix} \begin{bmatrix} E^+_{k_+}M' \\ -E^-_{k_-} \end{bmatrix} P'h = PMf^0, \tag{22}$$

for the density h with 8 scalar components. We write $f^0 = F^0|_\Gamma$ for the incident field on Γ. The preconditioning matrices P, P' will be chosen as constant diagonal matrices, and the scaling parameter r is $r = 1/\hat{k}$ in all our Dirac BIEs.

The well posedness of $\mathrm{DTP}(k_-, k_+, \alpha, \beta, \gamma)$ is equivalent to invertibility of $\begin{bmatrix} E^+_{k_+} & -ME^-_{k_-} \end{bmatrix}$, as a map from the direct sum of the ranges of $E^+_{k_+}$ and $E^-_{k_-}$. Consider also an auxiliary $\mathrm{DTP}(k_+, k_-, \alpha', \beta', \gamma')$, with the wavenumbers swapped, with an auxiliary Maxwell jump parameter α' and with two auxiliary Helmholtz jump parameters β', γ'. The duality result from [18, Prop. 8.5] shows that well posedness of $\mathrm{DTP}(k_+, k_-, \alpha', \beta', \gamma')$ is equivalent to invertibility of $\begin{bmatrix} E^+_{k_+}M' \\ -E^-_{k_-} \end{bmatrix}$, as a map onto the direct sum of the ranges of $E^+_{k_+}$ and $E^-_{k_-}$, with

$$M' = \mathrm{diag} \begin{bmatrix} 1/\alpha' & 1/\gamma' & \mathbf{1} & \hat{k} & 1/(\hat{k}\alpha'\beta') & \mathbf{1/(\alpha'\hat{k})} \end{bmatrix}. \tag{23}$$

The resulting Dirac BIE (22) has 12 free parameters

$$r, \beta, \gamma, \alpha', \beta', \gamma' \quad \text{and} \quad P' = \mathrm{diag} \begin{bmatrix} p'_1 & p'_2 & \boldsymbol{p'_{3:4}} & p'_5 & p'_6 & \boldsymbol{p'_{7:8}} \end{bmatrix} \tag{24}$$

to be chosen. We recall that $\alpha = \hat{k}^2$ for the non-magnetic Maxwell transmission problem that we want to solve. For r and P', any non-zero and finite complex numbers are allowed, although we have always used $r = 1/\hat{k}$ so far. Given P', we choose P so that

$$P(rM' + M)P' = I, \tag{25}$$

and set $N = PM$ and $N' = rM'P'$. This turns the Dirac BIE (22) into a second kind integral equation

$$h + (PE_{k_+}N' - NE_{k_-}P')h = 2Nf^0, \tag{26}$$

where we have used that $(E^\pm_k)^2 = E^\pm_k = \frac{1}{2}(I \pm E_k)$. The operator to invert on Γ is $I + G$, where G denotes the singular integral operator

$$PE_{k_+}N' - NE_{k_-}P' = P(E_{k_+}(rM') - ME_{k_-})P', \tag{27}$$

containing 30 scalar integral operators of double layer type, and 20 scalar integral operators of single layer type, according to (15). For a given choice of parameters, the operator G is computed using [18, Eqs. (131), (132)].

From the density h, obtained by solving (26), we compute the traces on Γ of the Dirac fields $F^\pm$ as

$$F^+|_\Gamma = E^+_{k_+}N'h \quad \text{and} \quad F^-|_\Gamma = -E^-_{k_-}P'h. \tag{28}$$

The fields $F^\pm$ in $\Omega^\pm$ are computed by instead using the corresponding non-singular (replacing $x \in \Gamma$ by $x \in \Omega^\pm$) versions of the Cauchy integrals $E^\pm_{k_\pm}$ in (28). Discarding the two auxiliary Helmholtz components in $F^\pm$ (which are 0 for Maxwell data f^0), and recalling (11), this yields $E^\pm$ and $H^\pm$. These field formulas are detailed in [17, Eqs. (28)–(31)]. Note that in computing H^+, the factor $\hat{k}$ from (11) cancels the factor $r = 1/\hat{k}$ in N' from (28), whereas this factor $1/\hat{k}$ remains in E^+. Note also that the minus sign in the second equation in (28) is contained in the field equations [17, Eqs. (28), (30)].

7

3.1. Dirac (A)

The Dirac parameters

$$\begin{bmatrix} r & \beta & \gamma & \alpha' & \beta' & \gamma' \end{bmatrix} = \begin{bmatrix} \frac{1}{\hat{k}} & \xi & a & \frac{1}{\hat{k}} & \frac{1}{\hat{k}} & \overline{a} \end{bmatrix},$$
$$P' = \operatorname{diag} \begin{bmatrix} 1 & \hat{k}^{1/2}(1+a)^{-1/2} & \boldsymbol{\hat{k}^{1/2}} & 1 & 1 & \boldsymbol{\frac{\hat{k}}{\hat{k}+1}} \end{bmatrix}, \tag{29}$$

were proposed in [18, Thm. 2.3], where $a = \hat{k}/|\hat{k}|$. Here the overline symbol denotes the complex conjugate and

$$\xi = 1 + i\delta \arg(\hat{k}) \tag{30}$$

is a tuning factor, set to $\xi = 1$ in [18] and further discussed below. The relations above then give

$$P = \begin{bmatrix} \frac{\xi}{\hat{k}^{-1}+\xi} & \hat{k}^{1/2}(1+a)^{-1/2} & \boldsymbol{\frac{\hat{k}^{1/2}}{2}} & \frac{1}{1+\overline{a}} & \frac{1}{1+\hat{k}^{-2}} & \boldsymbol{1} \end{bmatrix},$$
$$N = \begin{bmatrix} \frac{1}{1+\xi\hat{k}} & \frac{1}{\hat{k}^{1/2}}(1+a)^{-1/2} & \boldsymbol{\frac{1}{2\hat{k}^{1/2}}} & \frac{1}{1+a} & \frac{1}{1+\hat{k}^2} & \boldsymbol{1} \end{bmatrix}, \tag{31}$$
$$N' = \begin{bmatrix} 1 & \frac{1}{|\hat{k}|^{1/2}}(1+\overline{a})^{-1/2} & \boldsymbol{\frac{1}{\hat{k}^{1/2}}} & 1 & 1 & \boldsymbol{\frac{1}{1+\hat{k}}} \end{bmatrix}.$$

The main operator G from (27) is in general not compact, not even on smooth domains. However, we have that G is nilpotent modulo compact operators on smooth domains. This property is important for the efficiency of GMRES, since it implies that the only accumulation point for the spectrum of G is zero. The above choices of $r, \beta = 1, \alpha', \beta'$ ensure this through cancellations in the (1:2,3:4) and (7:8,5:6) blocks. The choices of γ, γ' were made only to avoid false eigenwavenumbers by chosing suitable complex arguments for them.

In [17, Sec. 5.1], we chose $\delta = 0.2/\pi$ in (30). This turns the complex argument of β slightly towards the argument of $\hat{k}$, which avoids false eigenwavenumbers in plasmonic scattering. The change is still small enough for G to be close to a nilpotent operator modulo compact operators on smooth Γ, so that iterative solvers converge rapidly. See Section 4. We refer to this Dirac BIE as Dirac (A), which performs well on any Lipschitz surface, of any genus, as long as $|\hat{k}|$ is bounded away from 0 and ∞. Throughout [18, 17], we only consider $|\hat{k}|$ which are not too large or small, and the choice for P' is then less important. In the present paper, we allow $\hat{k} \to \infty$, and then the parameters need to be chosen with more care, since Dirac (A) is no longer performing well.

4. Tuning and augmentation

We describe in this section some ideas for designing efficient BIEs in general, and Dirac BIEs in particular. A first step is to obtain Fredholm operators both (a) for the system to be solved and (b) for the field representation, by tuning the free parameters in the BIE. Recall that an operator is Fredholm if its null space is finite-dimensional and its range is closed and has finite codimension. An operator that fails to be Fredholm, for example a differential or hypersingular operator, may lead to "dense-mesh breakdown" in the computation, in the terminology of [31]. Even if the operators are Fredholm for each $k_- > 0$, but not uniformly as $k_- \to 0$, there may be a low-frequency breakdown in the computation.

The top three considerations in tuning Dirac BIEs are the following.

- The singular integral operator G should be close in norm to a nilpotent operator modulo compact operators on smooth Γ, to work well in an iterative solver. Our experience is that the choice $r = 1/\hat{k}$ is necessary for this.

- The complex arguments of $\beta/\hat{k}$, $\gamma/\hat{k}$, $\alpha'\hat{k}$, $\beta'\hat{k}$ and $\gamma'\hat{k}$ should be

$$\leq \pi - \arg(k_+/i) - \arg(k_-/i) \tag{32}$$

to avoid false eigenwavenumbers. When $k_\pm$ are on the real or imaginary axis, a strict inequality is required, and sometimes $\arg(-z)$ may replace $\arg(z)$, for z being one of the five

complex numbers above. We refer to [18, Props. 8.4-5 and Defn. 2.1] for details. False essential spectrum may appear when one of $\beta, \gamma, \alpha', \beta', \gamma'$ is in a compact subset of the negative real axis $(-\infty, 0)$. See Section 9.

The role of the tuning factor ξ from (30) in the Dirac BIEs is to slightly adjust parameters, not only β, but also α' and γ' in the Dirac BIEs presented below, to obtain a strict inequality in (32). This typically ensures that false eigenwavenumbers are avoided in plasmonic scattering, that is when $(\arg(k_-), \arg(k_+)) = (0, \pi/2)$ or $(\pi/2, 0)$.

- The coefficients in G, depending on P, P', N, N', should be uniformly bounded in the set of $k_\pm$ considered. For this, we note that it is sufficient but not necessary to have P, P', N, N' bounded. That it is needed to have N bounded is clear from the right-hand side in (26). Most importantly, N' and P' should be chosen so that (28) computes the fields at the correct scale. The generic scale for the fields in the eddy current regime is discussed in Section 5 below.

A second step in the design of efficient BIEs is to remove remaining finite-dimensional null spaces in the Fredholm maps. In an abstract setting, the typical situation is that finite-dimensional null spaces open up as a parameter $\lambda \to 0$, depending on the topology of Γ, causing a "topological low-frequency breakdown". See [7, 9, 12] for examples of this generic problem for BIEs. We remove such null spaces through augmentation. Recall from (5) that the typical construction of a BIE is to compose jump relations $g = B_\lambda F$ and a field representation $F = A_\lambda h$ to obtain a linear system

$$g = (I + G_\lambda)h = B_\lambda A_\lambda h. \tag{33}$$

Here both g and h belong to a suitable space of functions on Γ, but the domain of B_λ and the range of A_λ consist of a space of fields $F = F^\pm$ in $\Omega_\pm$ satisfying the differential equation, or equivalently a corresponding space of traces $F^\pm|_\Gamma$ on Γ. We assume that both A_λ and B_λ are Fredholm maps with index 0. In general both maps A_λ and B_λ may require augmentation. We refer to augmentation of the right factor, the field representation, as (R) augmentation, and to augmentation of the left factor, the jump relations, as (L) augmentation.

The logic behind the two types of augmentations is quite different. We therefore discuss them separately, starting with two elementary but illustrative examples of augmentation of BIEs for Helmholtz boundary value problems, with no aim for completeness or full proofs. It is clear from these examples that (R) augmentation is required when we have null densities $h + G_0 h = 0$ corresponding to zero fields $F = A_0 h = 0$. Otherwise (L) augmentation is required in order to obtain an invertible system.

Example 1 (Exterior Dirichlet problem). Consider the Dirichlet problem $u|_\Gamma = g$ for $\Delta u + k^2 u = 0$ in Ω_-, with standard Sommerfeld radiation condition at ∞, for k in a neighbourhood of 0. This has a unique solution u for all k in a neighbourhood of 0, including 0, so no (L) augmentation is needed. Using the standard double layer potential representation of u however, leads to a BIE $h + K_k^{\nu'} h = 2g$, which at $k = 0$ has a null space spanned by constant functions h. We resolve this problem by using an (R) augmented field representation

$$u(x) = \int_\Gamma \nabla \Phi_k(y - x) \cdot \nu(y) h(y) d\Gamma(y) + \Phi_k(x - p) \int_\Gamma h d\Gamma(y), \qquad x \in \Omega_-, \tag{34}$$

with some fixed $p \in \Omega_+$. In dimension two, the fundamental solution $\Phi_k(x - p) = (i/2) H_0^{(1)}(k|x - p|)$ uses the Hankel function and needs to be divided by $\log(k)$ in the second term in (34). This leads to the (R) augmented BIE $h + K_k^{\nu'} h + b_k(ch) = 2g$ with the finite-rank operator $b_k c$ added, where $b_k = \Phi_k(\cdot - p)|_\Gamma$ and $ch = \int_\Gamma h d\Gamma$. This is stably solvable for h, for all k near 0, and the field u is computed from the augmented representation (34). This can be seen as a rank-1 version of the combined field integral equation [6, Eq. (3.25)], which only removes the false eigenwavenumber at $k = 0$. It can also be seen as a generalization to $k \neq 0$ of the standard treatment for $k = 0$ in [15, p. 345].

In an abstract setting, (R) augmentation can be described as follows. We consider a parameter $\lambda \to 0$, and for each fixed $\lambda \neq 0$ we compose jump relations B_λ and field representations A_λ as in (33) to obtain a system

$$h + G_\lambda h = g. \tag{35}$$

We assume that free parameters have been tuned so that $I + G_\lambda$ is invertible for each $\lambda \neq 0$, but that it is merely a Fredholm map at $\lambda = 0$. Assume for simplicity that the null space $\mathsf{N}(I + G_0)$ is one-dimensional. If B_0 is invertible and the null space for $I + G_0$ comes from the field representation A_0, then we identify a functional c that is non-zero on $\mathsf{N}(A_0) = \mathsf{N}(I + G_0)$ and a field/solution F_λ for each parameter λ, such that $F_\lambda \to F_0$ where F_0 does not belong to the range $\mathsf{R}(A_0)$. Let $b_\lambda = B_\lambda F_\lambda$ be the corresponding boundary datum. The obtained (R) augmented BIE uses the field representation $F = A_\lambda h + F_\lambda(ch)$, where the density h now solves the (R) augmented system $(I + G_\lambda + b_\lambda c)h = g$.

Example 2 (Interior Neumann problem). Consider the Neumann problem $\partial_\nu u|_\Gamma = g$ for $\Delta u + k^2 u = 0$ in Ω_+, for k in a neighbourhood of 0. We have a unique solution u, except at $k = 0$, and an (L) augmentation is required. To note is that

$$\int_\Gamma g d\Gamma = -k^2 \int_{\Omega_+} u dx, \tag{36}$$

which forces $\int_{\Omega_+} u dx = 0$ if $k \neq 0$ and $\int_\Gamma g d\Gamma = 0$. The standard single layer potential $u(x) = \int_\Gamma \Phi_k(x - y)h(y)d\Gamma(y)$, $x \in \Omega_+$, gives a representation of all solutions u in Ω_+ and needs no (R) augmentation, but leads to the BIE $h - K_k^\nu h = 2g$, which for $k = 0$ has a one-dimensional null space. For $k \neq 0$, define the functional

$$c_k h = \int_{\Omega_+} u dx = -\frac{1}{k^2} \int_\Gamma g d\Gamma = -\frac{1}{2k^2} \int_\Gamma (h - K_k^\nu h) 1 d\Gamma = \int_\Gamma h w_k d\Gamma, \tag{37}$$

with weight function $w_k = (K_0^{\nu'} 1 - K_k^{\nu'} 1)/(2k^2)$. The last equality in (37) follows from duality and $K_0^{\nu'} 1 = -1$. By Taylor expansion of $\nabla \Phi_k$, this computation of w_k can be stabilized, and for $k \neq 0$ our BIE is seen to be equivalent to

$$h - K_k^\nu h + b(c_k h) = 2g - k^{-2} b \int_\Gamma g d\Gamma. \tag{38}$$

Choosing the constant function $b = 1$ on Γ, the operator $I - K_k^\nu + bc_k$ is well-conditioned for all k near 0, and the previous low-frequency breakdown has moved to the simpler computation of the second term on the right-hand side.

In an abstract setting, (L) augmentation can be described as follows. Consider $I + G_\lambda = B_\lambda A_\lambda$ as $\lambda \to 0$ as above, but assume now that the field representation A_0 is invertible but that B_0 has a one-dimensional null space. We identify a scalar equation

$$c_\lambda h = d_\lambda g, \tag{39}$$

which follows from $h + G_\lambda h = g$ for $\lambda \neq 0$, but may fail at $\lambda = 0$. The equation (39) often appears by rescaling one scalar component of the jump relations so that c_λ is normalized. We assume that $c_\lambda \to c_0$ as $\lambda \to 0$, where $c_0 \neq 0$ on $\mathsf{N}(I + G_0)$. Typically $d_\lambda g$ will not stay bounded as $\lambda \to 0$, unless we assume that data satisfy $d_\lambda g = 0$, in which case we speak of a *homogeneous* (L) augmentation. Choosing an auxiliary function $b \notin \mathsf{R}(A_0) = \mathsf{R}(I + G_0)$, we obtain the (L) augmented BIE with system $(I + G_\lambda + bc_\lambda)h = g + b(d_\lambda g)$ and field representation as before.

For Dirac BIEs, the factorization $I + G_\lambda = B_\lambda A_\lambda$ is given by (22). Following the ideas presented in this section, we obtain the augmentations for our Dirac BIE that are stated in Sections 6 and 7. The derivation of these augmentations are found in Appendix A. It should be noted that Dirac (A∞) only requires a single (L) augmentation for the Dirichlet eigenfield, regardless of the genus of Γ, whereas Dirac (B) for Γ of genus $g \geq 0$ requires $1 + g$ (R) augmentations and $1 + g$ (L) augmentations for the Dirichlet and Neumann eigenfields, and an (L) augmentation of a Helmholtz eigenfield.

Remark 2. An alternative technique for augmenting a BIE in the form $(I + G_\lambda)h = g$ is to add equations and unknowns. Consider

$$\begin{bmatrix} I + G_\lambda & B_\lambda \\ C_\lambda & D_\lambda \end{bmatrix} \begin{bmatrix} h \\ a \end{bmatrix} = \begin{bmatrix} g \\ d_\lambda g \end{bmatrix}. \tag{40}$$

With only one extra equation and unknown in (40), and with $D_\lambda = -1$, the elimination of a shows that (40) is equivalent to the additive (L) augmentation described above.

Now (40) can be converted to Fredholm second kind block triangular form, which is better suited for an iterative solver, using

$$\begin{bmatrix} I & B_\lambda \\ C_\lambda & D_\lambda \end{bmatrix} \tag{41}$$

as a left- or right preconditioner in (40). The inverse of (41) can be efficiently applied via the solution of a system involving the Schur complement of I. See [14, Sec. 4.1] for an example. Nevertheless, we find that our additive augmentations are easier to work with than this more traditional technique involving extra equations and preconditioners.

Augmentations have been frequently used in literature. Most of these concern the simpler problem of augmenting static Laplace or biharmonic problems, which corresponds to augmenting only $I + G_0$, that is, $I + G_\lambda$ at $\lambda = 0$. Static homogeneous (L) augmentation appears in [24, p. 257]. Static (R) augmentation appears in [14, Eqs. (11),(23)]. Non-static inhomogeneous (L) augmentation appears in [9, Rem. 1].

5. Eddy current eigenfields

Assume that the incident fields E^0 and H^0 have magnitude of order 1 on Γ. Then the transmitted magnetic field H^+ is of order 1 since Ω_+ is non-magnetic, and the scattered electric field E^- is also of order 1, assuming that we are in the eddy current regime. The transmitted electric field E^+ satisfies $\nabla \times E^+ = ik_- H^+$, $\nabla \cdot E^+ = 0$ and

$$\nu \cdot E^+ = \hat{k}^{-2} \nu \cdot (E^- + E^0), \tag{42}$$

which shows that E^+ is of order $\max(k_- L, |\hat{k}^{-2}|)$ in the generic scattering situation. From this we conclude that the magnitude of the eddy current

$$J = \sigma E^+ = \mathrm{Re}(k_+^2/(i\eta_0 k_-))E^+ \tag{43}$$

is of order $\max(|k_+|^2 L, k_-)$, and the scattered magnetic field H^- is of order $\max((|k_+|L)^2, k_- L)$.

The incident field that we use in our numerical examples is a sum of the two lowest order axially symmetric spherical vector waves [22, Eq. (7)]

$$E^0(x) = G(x) + k_-^{-1} \nabla \times G(x), \qquad H^0(x) = -iE^0(x). \tag{44}$$

Here $G(x) = \sqrt{3/(8\pi)} j_1(k_- |x|)\rho |x|^{-1} \boldsymbol{\theta}$ and j_1 is the spherical Bessel function of order 1.

We see two types of eigenfields appearing in the eddy current regime as $k_- \to 0$, which generalize the classical (exterior) Dirichlet and Neumann eigenfields (or Dirichlet and Neumann vector fields in the terminology of [5]) in PEC scattering, and where the magnitude of the fields can differ drastically from those described above. As discussed below, the Dirichlet eigenfield is non-physical in the sense that it cannot be excited by sources in Ω_-, whereas the Neumann eigenfield, see (46) and Figure 2(g,h,i) for ordinary conductors, indeed can be excited by such sources, and is of physical origin and not an artifact of any field representation. We say that there exists an eigenfield in the eddy current regime if there are incident fields such that

$$\frac{\|E^+\|/\max(k_- L, |\hat{k}^{-2}|) + \|E^-\| + \|H^+\| + \|H^-\|}{\|E^0\| + \|H^0\|} \to \infty, \tag{45}$$

as $k_- \to 0$ along a curve in the (k_-, k_+) plane, contained in the eddy current regime. Here the norm $\| \cdot \|$ of a vector field on Γ is the sum of the $H^{-1/2}(\Gamma)$ norm of its normal component and

the $H^{-1/2}(\mathrm{curl}, \Gamma)$ norm of its tangential part. See [18, Eq. (65)]. The eigenfield is defined to be the limit of $\{E^+, E^-, H^+, H^-\}$, normalized suitably. In the sum in (45), we have scaled each of the four fields $\{E^+, E^-, H^+, H^-\}$ by the generic size of the corresponding measurable field $\{E^+, E^0 + E^-, H^+, H^0 + H^-\}$.

The classical exterior Dirichlet eigenfield is a divergence- and curl-free electric field in Ω_- which is normal on Γ and decays at ∞, resulting from a net charge in Ω_+. However, Ω_+ is assumed to have zero net charge and thus such eigenfields cannot be excited by sources located in Ω_-. Since we only assume sources in Ω_-, we will not see any Dirichlet eigenfields appearing. Our augmentations of null spaces related to the Dirichlet eigenfields build on (8). This condition excludes Dirichlet eigenfields E^-, since the maximum principle applied to the electric potential shows that $\nu \cdot E^-$ cannot change sign, which forces E^- to be zero in Ω^-.

The classical exterior Neumann eigenfield is a divergence- and curl-free magnetic field in Ω_- which is tangential on Γ and decays at ∞, resulting from an electric current on the surface of genus ≥ 1 of a superconductor. For a torus, the current is in the θ direction, and the Neumann eigenfield is in the τ direction on Γ. For an ordinary conductor, we see the Neumann eigenfield appearing in (7) as $k_- \to 0$ in the eddy current regime, as follows. Instead of E^+ we consider the auxiliary field $\widetilde{E}^+ = E^+ / \max(k_- L, |\hat{k}^{-2}|)$, since in the generic scattering situation the field $\widetilde{E}^+$ is of order 1. Setting $E^0 = H^0 = 0$, the first equation in (7) shows that $\nu \times E^- = 0$, since $E^+ \to 0$ as $k_- \to 0$ in the eddy current regime. This forces $E^- = 0$ since E^- is a divergence- and curl-free vector field in Ω_- and satisfies (8). From the jump relation $\nu \cdot E^+ = \hat{k}^{-2}\nu \cdot E^-$, which follows from the second equation in (7), we conclude that $\nu \cdot \widetilde{E}^+ = 0$. Therefore $\widetilde{E}^+$, as well as the eddy current $J = \sigma E^+$, is a divergence- and curl-free vector field in Ω_+ with vanishing normal component at Γ. Finally the magnetic field H is a divergence-free vector field in $\mathbf{R}^3$ solving

$$\nabla \times H = \begin{cases} \eta_0 J, & \text{in } \Omega_+, \\ 0, & \text{in } \Omega_-, \end{cases} \tag{46}$$

which follows from (7) since $-ik_+\hat{k} = \eta_0\sigma$. To summarize, the De Rham cohomology space $H^1(\Omega_+)$, see for example [26, Sec. 10.6], parametrizes the Neumann eigenfields. More precisely the eddy current $J = \sigma E^+$ is a divergence- and curl-free field which is tangential on Γ, and the associated magnetic field is obtained by applying the Biot–Savart operator to $\eta_0 J$. Note from (46) for the Neumann eigenfield that H and J are independent of σ for all ordinary conductors with $0 < \sigma < \infty$. In contrast to the Dirichlet eigenfields, the Neumann eigenfields can be excited by sources in Ω_-. Thus some ill-conditioning is inevitable in any BIE since the Neumann eigenfield is a physical eigenfield. By an inhomogeneous (L) augmentation similiar to Example 2, we shall obtain a well-conditioned system and field representation, locating the ill-conditioning to the simpler computation of the right hand side for the system. In Section 8, we demonstrate that the Neumann eigenfield in an ordinary conductor can be excited by the incident field

$$E^0(x) = ic_2 H_1^{(1)}(k_-\rho)\boldsymbol{\theta}, \qquad H^0(x) = c_2 H_0^{(1)}(k_-\rho)\boldsymbol{z}, \tag{47}$$

normalized with $c_2 = 1/|H_1^{(1)}(k_-)|$ and where $H_n^{(1)}$ is the first kind Hankel function of order n. This field can in principle be generated by a thin wire along the z-axis made of a material with high relative permeability $\mu_r \gg 1$. By closing the wire in a large loop and exciting a magnetic field inside the wire by a coil around the wire, a field like (47) will be incident on Γ.

An important point is that the Neumann eigenfield obtained in the PEC approximation is not the eigenfield appearing in ordinary conductors. The difference is illustrated in Figure 2 where (g,h,i) shows the Neumann eigenfield appearing in ordinary conductors. Note that the H field penetrates into Ω_+ and that the eddy current flows in the interior of Ω_+, unlike the Neumann eigenfield for superconductors shown in Figure 2(a,b,c), where the current flows on the surface Γ, as shown qualitatively in Figure 2(a). Figure 2(d,e,f) shows an intermediate eigenfield in the case when the scaled conductivity grows inversely proportional to k_- as $k_- \to 0$ so that the skin depth is fixed in the sense that $k_+ = 10(1 + i)$. Here we see how J and H begin to be expelled from Ω_+.

Note that the ill-posedness of the MTP in the eddy current regime for Γ of genus 1, due to the existence of Neumann eigenfields, does not contradict conservation of energy. Since we consider total permittivities ϵ_+ that are imaginary, there will be no transmitted electric energy in Ω^+, only
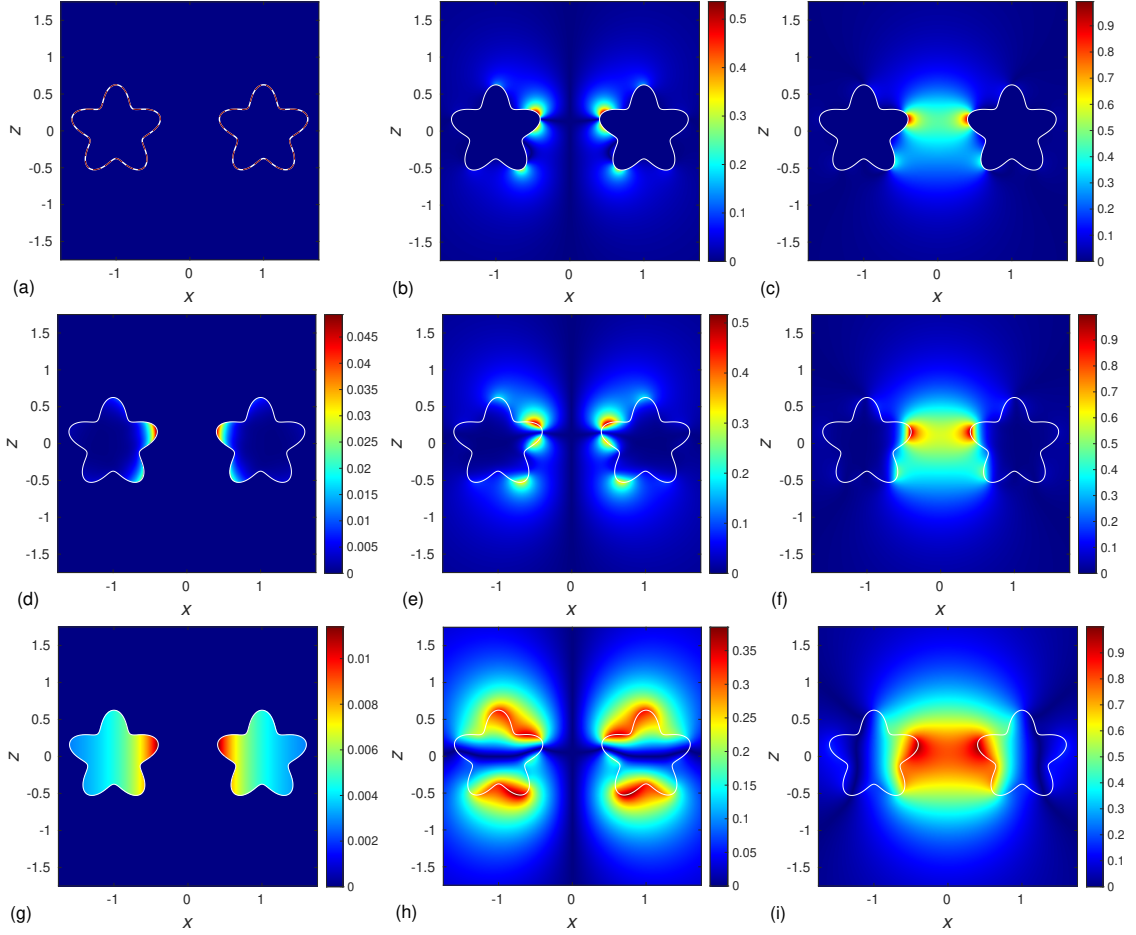
Figure 2: Neumann eigenfields of the "starfish torus" (71), normalized so that $\max|H| = 1$; (a,d,g) eddy current $|J_\theta|$; (b,e,h) $|H_\rho|$; (c,f,i) $|H_z|$; (a,b,c) eigenfield for a superconductor; (d,e,f) borderline eddy current-PEC eigenfield at $k_+ = 10(1 + i)$; (g,h,i) eigenfield of an ordinary conductor.

a large magnetic energy. However, to excite the Neumann eigenfield requires an incident field like (47), which requires a large power to be produced by the coil.

6. Dirac (A∞)

For the remainder of this paper, we choose unit of length so that L is of order 1. In [17], it was demonstrated that Dirac (A) works well near the quasi-static limit $k_\pm \to 0$, provided $|k_+|$ and k_- are comparable in size. In this section, we first formulate a Dirac BIE, referred to as (A∞), that, after augmentation, is intended to be used in the eddy current regime (4). The resulting BIE, referred to as (A∞-aug), is insensitive to the genus of Γ and builds on (29), but differs in the choices of α', β' and the preconditioning P'. It is demonstrated in Section 8 that Dirac (A∞-aug) performs well when the Neumann eigenfields are excited.

Dirac (A∞) is defined by the parameters

$$
\begin{bmatrix} r & \beta & \gamma & \alpha' & \beta' & \gamma' \end{bmatrix} = \begin{bmatrix} \frac{1}{\hat{k}} & \xi & a & \frac{1}{|\hat{k}|\hat{k}} & \overline{a} & \overline{a} \end{bmatrix},
$$

$$
P = \begin{bmatrix} \frac{\hat{k}^2}{(|\hat{k}|+(\hat{k}\xi)^{-1})\langle\sigma\rangle} & \frac{\hat{k}}{(1+a)\langle\sigma\rangle} & \frac{\hat{k}}{2\langle\sigma\rangle} & \frac{1}{1+\overline{a}} & \frac{1}{1+\hat{k}^{-2}} & \frac{1}{1+\overline{a}} \end{bmatrix},
$$

$$
P' = \begin{bmatrix} \frac{\langle\sigma\rangle}{\hat{k}^2} & \langle\sigma\rangle & \langle\sigma\rangle & 1 & 1 & 1 \end{bmatrix}, \tag{48}
$$

$$
N = \begin{bmatrix} \frac{\hat{k}^2}{(|\hat{k}|\hat{k}\xi+1)\langle\sigma\rangle} & \frac{1}{(1+a)\langle\sigma\rangle} & \frac{1}{2\langle\sigma\rangle} & \frac{\overline{a}}{1+\overline{a}} & \frac{1}{1+\hat{k}^2} & \frac{1}{1+\overline{a}} \end{bmatrix},
$$

$$
N' = \begin{bmatrix} \frac{\langle\sigma\rangle}{a\hat{k}} & \frac{\langle\sigma\rangle}{|\hat{k}|} & \frac{\langle\sigma\rangle}{\hat{k}} & 1 & 1 & \overline{a} \end{bmatrix}.
$$

13

Here $a = \hat{k}/|\hat{k}|$, ξ is as in (30), and

$$\langle \sigma \rangle = 1 + |k_+ \hat{k}|. \tag{49}$$

We have the following behaviour of Dirac (A∞):

- The coefficients in G of Dirac (A∞) are uniformly bounded and, similar to G of Dirac (A), the G of Dirac (A∞) is close to a nilpotent operator modulo compact operators on smooth Γ due to cancellations in blocks (1:2,3:4) and (7:8,5:6). Furthermore, the norm of the (5:8,1:4) block is of order $k_- \langle \sigma \rangle$, whereas the norm of the (1:4,5:8) block is of order $|k_+ \hat{k}/\langle \sigma \rangle|$.

- All entries in N are bounded. Inserting N' and P' into (28), it is seen that

$$\|E^\pm|_\Gamma\| \lesssim \|h\| \quad \text{and} \quad \|H^\pm|_\Gamma\| \lesssim \langle \sigma \rangle \|h\|. \tag{50}$$

  This possibility of having large transmitted and scattered fields, even if the density h is not large, explains why (A∞) is able to accurately compute the fields when the Neumann eigenfields are excited.

- For fixed $k_\pm \neq 0$, the choice of $\beta, \gamma, \alpha', \beta', \gamma'$ guarantees invertibility of $I + G$. The limit operator $I + G_0$ as $k_\pm \to 0$ in the eddy current regime is a Fredholm operator of index zero, and it has nullity 1 regardless of the genus of Γ. See Appendix A. At high conductivities, this analysis breaks down, but computations suggest that the null space remains one-dimensional.

Following Section 4, we make one (L) augmentation to remove the Dirichlet eigenfield. Recall from Section 5 that this eigenfield cannot be excited by sources in Ω_-, and therefore a homogeneous (L) augmentation is appropriate. For details we refer to Appendix A. The field representation for Dirac (A∞) fails to be a Fredholm map as $k_- \to 0$, as discussed in Section 8.5, and (R) augmentations are therefore not applicable.

6.1. Dirac (A∞-aug)

To remove the Dirichlet eigenfield we make the homogeneous (L) augmentation of Dirac (A∞)

$$c_D^1 h = \fint_\Gamma (E_{k_-}^- P' h)_6 d\Gamma,$$
$$b_D^1 = \begin{bmatrix} 0 & 0 & \mathbf{0} & 0 & 1 & \mathbf{0} \end{bmatrix}^T. \tag{51}$$

Here $\fint_\Gamma f d\Gamma$ denotes the average value of a function f on Γ. We thus obtain a Dirac (A∞-aug), intended for Γ of any genus. Given f^0, we solve the augmented system

$$h + Gh + b_D^1(c_D^1 h) = 2N f^0, \tag{52}$$

with G, c_D^1, b_D^1 from (27), (51), and the parameters (48) above. This yields h, from which we compute the fields using (28).

7. Dirac (B)

Recall that we are using unit of length so that L is of order 1. In this section, we first formulate a Dirac BIE, referred to as (B), for the MTP$(k_-, k_+, \hat{k}^2)$ that, after augmentation, is intended to be used in the eddy current regime (4). Dirac (B) is radically different in the choices of parameters from both Dirac (A) and Dirac (A∞), and is designed to compute each of the fields $E^\pm, H^\pm$ accurately when the Neumann fields are not excited. It is defined by the parameters

$$\begin{aligned}
\begin{bmatrix} r & \beta & \gamma & \alpha' & \beta' & \gamma' \end{bmatrix} &= \begin{bmatrix} \frac{1}{\hat{k}} & \frac{\hat{k}}{|\hat{k}|^2} & \frac{\hat{k}^2}{\xi} & \frac{1}{\xi} & \frac{1}{\hat{k}} & \frac{1}{\xi} \end{bmatrix}, \\
P &= \begin{bmatrix} \frac{1}{\xi \hat{k}^{-1} + a^{-2}} & \frac{\hat{k}}{\xi+1} & \frac{\mathbf{\hat{k}}}{\mathbf{2}} & \frac{\hat{k}^2}{\langle \sigma \rangle} \frac{1}{1+\xi \hat{k}^{-2}} & \frac{\hat{k}^2}{\langle \sigma \rangle} \frac{1}{\xi + \hat{k}^{-1}} & \frac{\mathbf{1}}{\mathbf{1+\xi \hat{k}^{-2}}} \end{bmatrix}, \\
P' &= \begin{bmatrix} 1 & 1 & \mathbf{1} & \frac{\langle \sigma \rangle}{\hat{k}^2} & \frac{\langle \sigma \rangle}{\hat{k}} & \mathbf{1} \end{bmatrix}, \\
N &= \begin{bmatrix} \frac{1}{1+\xi a^2/\hat{k}} & \frac{1}{\xi+1} & \frac{\mathbf{1}}{\mathbf{2}} & \frac{\xi}{\langle \sigma \rangle} \frac{1}{1+\xi \hat{k}^{-2}} & \frac{1}{\langle \sigma \rangle} \frac{1}{\xi + \hat{k}^{-1}} & \frac{\mathbf{1}}{\mathbf{1+\xi \hat{k}^{-2}}} \end{bmatrix}, \\
N' &= \begin{bmatrix} \frac{\xi}{\hat{k}} & \frac{\xi}{\hat{k}} & \frac{\mathbf{1}}{\mathbf{\hat{k}}} & \frac{\langle \sigma \rangle}{\hat{k}^2} & \frac{\xi \langle \sigma \rangle}{\hat{k}^2} & \frac{\mathbf{\xi}}{\mathbf{\hat{k}^2}} \end{bmatrix},
\end{aligned} \tag{53}$$

where $a = \hat{k}/|\hat{k}|$, ξ is as in (30), and $\langle\sigma\rangle$ is as in (49). We have the following behaviour of Dirac (B):

- The coefficients in G are uniformly bounded for all $|\hat{k}| \gtrsim 1$. The operator G is close to a nilpotent operator modulo compact operators on smooth Γ, but unlike Dirac (A) and (A∞), this is due to cancellations mainly in blocks (3:4,1:2) and (5:6,7:8). Furthermore, the norm of the (5:8,1:4) block is of order $|k_+\hat{k}/\langle\sigma\rangle|$, whereas the norm of the (1:4,5:8) block is of order $k_-\langle\sigma\rangle$.

- All entries in P', N, N' are uniformly bounded for all $|\hat{k}| \gtrsim 1$, and N' is adapted to the generic sizes of the fields, as discussed in Section 5, so that

$$(|\hat{k}^2|/\langle\sigma\rangle)\|E^+|_\Gamma\|, \quad \|E^-|_\Gamma\|, \quad \|H^+|_\Gamma\|, \quad \|H^-|_\Gamma\| \tag{54}$$

  are all $\lesssim \|h\|$.

- For fixed $k_\pm \neq 0$, the choice of $\beta, \gamma, \alpha', \beta', \gamma'$ guarantees invertibility of $I + G$. The limit operator $I + G_0$ as $k_- \to 0$ in the eddy current regime is a Fredholm operator of index zero, but its nullity depends on k_+ as well as on the genus of Γ. See Appendix A.

Following Section 4, we make a number of augmentations. First the field representation requires one or two (R) augmentations, depending on the genus of Γ, to become well-conditioned. Once this is done, one or two (L) augmentations are needed to remove the Dirichlet eigenfield and the null space associated with the Neumann eigenfield. It is only the Neumann eigenfield which can be excited by Maxwell sources in Ω_-, so that an inhomogeneous (L) augmentation is needed. A final (L) augmentation is also needed to remove an eigenfield which is present in the Dirac equation, but which is outside the Maxwell equations. For details we refer to Appendix A.

7.1. Dirac (B-aug0)

Consider Γ of genus 0. We first make an (R) augmentation

$$
\begin{aligned}
c_D^R h &= \fint_\Gamma h_6 d\Gamma, \\
b_D^R &= 2N E_{k_-}^- e_6,
\end{aligned}
\tag{55}
$$

where $e_6 = \begin{bmatrix} 0 & 0 & \mathbf{0} & 0 & 1 & \mathbf{0} \end{bmatrix}^T$, which has the effect of adding the Dirichlet eigenfield to the field representation. That field is missing in Dirac (B). This is needed to avoid a null space for the system. But since the Dirichlet eigenfield cannot be excited by sources in Ω_-, we also make a homogeneous (L) augmentation

$$
\begin{aligned}
c_D^2 h &= \fint_\Gamma (E_{k_-}^-(P'h + e_6(c_D^R h)))_6 d\Gamma, \\
b_D^2 &= e_1,
\end{aligned}
\tag{56}
$$

where $e_1 = \begin{bmatrix} 1 & 0 & \mathbf{0} & 0 & 0 & \mathbf{0} \end{bmatrix}^T$, which again removes the Dirichlet eigenfield. The two augmentations $b_D^R c_D^R$ and $b_D^2 c_D^2$ together make the system stably solvable when $k_+\hat{k} \gtrsim 1$. When $k_+\hat{k} \ll 1$ we also have a second eigenfield for the DTP. This field comes from one of the auxiliary HTPs, and we make a homogeneous (L) augmentation

$$
\begin{aligned}
c_H^1 h &= \fint_\Gamma (E_{k_+}^+ \hat{k} N' h)_1 d\Gamma, \\
b_H^1 &= \begin{bmatrix} 0 & 0 & \mathbf{0} & 0 & 1 & \mathbf{0} \end{bmatrix}^T.
\end{aligned}
\tag{57}
$$

We thus obtain a Dirac BIE, referred to as (B-aug0), intended for Γ of genus 0. Given f^0, we solve the augmented system

$$h + Gh + (b_D^R c_D^R + b_D^2 c_D^2 + \chi b_H^1 c_H^1)h = 2N f^0, \tag{58}$$

with G, $b_D^R c_D^R$, $b_D^2 c_D^2$ and $b_H^1 c_H^1$ from (27), (55), (56) and (57) using the parameters (53). Here

$$\chi = \begin{cases} 0, & |k_+\hat{k}| \gtrsim 1, \\ 1, & |k_+\hat{k}| \ll 1, \end{cases} \tag{59}$$

but numerically $\chi = 1$ seems to work in both cases. This yields h, from which we compute the fields using the augmented field representation

$$\begin{aligned} F^+|_\Gamma &= E_{k_+}^+ N' h, \\ F^-|_\Gamma &= -E_{k_-}^- (P'h + e_6(c_D^R h)). \end{aligned} \tag{60}$$

7.2. Dirac (B-aug1)

Consider an axially symmetric Γ of genus 1. (The construction in this section generalizes to arbitrary Γ of genus 1, if the τ and θ directions are suitably defined.) As for genus 0 we make the augmentations $b_D^R c_D^R$ and $b_D^2 c_D^2$ to remove the Dirichlet eigenfield. But for genus 1, we also need to make an (R) augmentation

$$\begin{aligned} c_N^R h &= \oint_\Gamma h_8 d\Gamma, \\ b_N^R &= 2\frac{\langle\sigma\rangle}{\hat{k}^2} P E_{k_+}^+ e_8, \end{aligned} \tag{61}$$

which has the effect of adding the Neumann eigenfield to the field representation. That field is also missing in Dirac (B). This gives the field representation

$$\begin{aligned} F^+|_\Gamma &= E_{k_+}^+ \left(N'h + \frac{\langle\sigma\rangle}{\hat{k}^2} e_8(c_N^R h)\right), \\ F^-|_\Gamma &= -E_{k_-}^- (P'h + e_6(c_D^R h)). \end{aligned} \tag{62}$$

We use $e_8 = \begin{bmatrix} 0 & 0 & 0 & 0 & 0 & 0 & 0 & 1 \end{bmatrix}^T$, which seems to work numerically, but the derivation in Appendix A uses e_8 with the θ component on Γ of the interior Neumann eigenfield in its last component.

For $k_+\hat{k} \ll 1$, we need to adjust the HTP augmentation $b_H^1 c_H^1$ to (62), and we set

$$\begin{aligned} c_H^2 h &= \oint_\Gamma \left(E_{k_+}^+ \left(\hat{k}N'h + \frac{\langle\sigma\rangle}{\hat{k}} e_8(c_N^R h)\right)\right)_1 d\Gamma, \\ b_H^2 &= \begin{bmatrix} 0 & 0 & \mathbf{0} & 0 & 1 & \mathbf{0} \end{bmatrix}^T. \end{aligned} \tag{63}$$

What remains is the more subtle inhomogeneous (L) augmentation of the Neumann eigenfield. As discussed in Section 5, the MTP is ill-posed in itself due to the presence of the Neumann eigenfield, but we make an inhomogeneous (L) augmentation that makes the system well-conditioned at the expense of adding an unbounded functional d_N^1 to the right-hand side. Let

$$\begin{aligned} c_N^1 h &= \oint_\Gamma \left(E_{k_+}^+ ((\hat{k}^2/\langle\sigma\rangle)N' + e_8 c_N^R)h\right)_8 w d\Gamma \\ &\quad + \frac{\hat{k}^2}{\langle\sigma\rangle} \oint_\Gamma \left(E_{k_-}^- P'h_{1:5}\right)_8 w d\Gamma + \frac{\hat{k}^2}{\langle\sigma\rangle} \oint_\Gamma \frac{1}{2}\left((E_0 - E_{k_-})h_{7:8}\right)_8 w d\Gamma, \\ b_N^1 &= \begin{bmatrix} 0 & 0 & 0 & 0 & 0 & 0 & 0 & 1 \end{bmatrix}^T = e_8, \\ d_N^1 f^0 &= \frac{\hat{k}^2}{\langle\sigma\rangle} \oint_\Gamma (f^0)_8 w d\Gamma, \end{aligned} \tag{64}$$

where $w = \tau \cdot H|_\Gamma$ is a weight function discussed below, and H denotes an exterior PEC Neumann eigenfield. Although the factor $\hat{k}^2/\langle\sigma\rangle$ makes d_N^1 unbounded, it turns out that $d_N^1 f^0$ stays bounded by f^0 unless the Neumann eigenfield is excited. More precisely, $d_N^1 f^0 / \max_\Gamma |f^0|$, measures how

much of the Neumann eigenfield will be excited. Indeed, an application of Stokes' theorem shows that

$$d_N^1 f^0 = \frac{ik_+ \hat{k}}{\langle\sigma\rangle|\Gamma|} \int_{\Omega_-} H^0 \cdot H dx, \tag{65}$$

where $|\Gamma|$ denotes the area of Γ and H^0 is, as before, the incident magnetic field.

The equation $c_N^1 h = d_N^1 f^0$ is seen to be equivalent to continuity of the θ component of the electric field across Γ, and normalized with the generic size of E^+. See Appendix A. We denote by $h_{1:5}$ the density h with components 6:8 set to zero, and likewise $h_{7:8}$ denotes the density h with components 1:6 set to zero. For this augmentation to work, it is essential to use a specific positive weight function w: the τ-component of the exterior PEC Neumann eigenfield, normalized so that $\oint_\Gamma w d\Gamma = 1$. The weight function can be computed as $w = \theta \cdot f$, where f is the solution to the size 2×2 block eigenfunction equation

$$(\boldsymbol{I} + \boldsymbol{M}_0)f = 0, \tag{66}$$

and $\boldsymbol{M}_0$ is the static magnetic dipole operator (18). Equivalently, and perhaps better from a numerical point of view, w can be computed as

$$w = \tau \cdot H_0 + K_0^\tau \psi, \tag{67}$$

where ψ is the solution to the single block Fredholm second kind integral equation

$$(I + K_0^\nu)\psi = -\nu \cdot H_0, \tag{68}$$

which can be solved iteratively. Note also that the system in (68) is half the size of the system (66). Here K_0^τ is defined as K_0^ν, but with $\nu(x)$ replaced by $\tau(x)$, and H_0 denotes the magnetic field produced by a steady current in a circular wire around Ω_+ (or any computable divergence- and curl-free vector field in Ω_- which is not a gradient field).

In total, we obtain a Dirac BIE referred to as (B-aug1) and intended for Γ of genus 1. Given f^0, we solve the augmented system

$$h + Gh + (b_D^R c_D^R + b_D^2 c_D^2 + b_N^R c_N^R + b_N^1 c_N^1 + \chi b_H^2 c_H^2)h = 2Nf^0 + b_N^1(d_N^1 f^0), \tag{69}$$

with G, $b_D^R c_D^R$, $b_D^2 c_D^2$, $b_N^R c_N^R$, $b_N^1 c_N^1 d_N^1$, $b_H^2 c_H^2$, from (27), (55), (56), (61), (64), (63) using the parameters (53). This yields h, from which we compute the fields using (62).

8. Numerical examples

The properties of Dirac (A∞-aug) from Section 6.1 and (B-aug0/1) from Sections 7.1 and 7.2 are now illustrated in a series of numerical examples involving two objects Ω_+ with axially symmetric surfaces:

- The "rotated starfish" has a surface Γ of genus 0, with generating curve

$$r(s) = (1 + 0.25\sin(5s))(\cos(s), \sin(s)), \qquad s \in [-\pi/2, \pi/2], \tag{70}$$

  and generalized diameter $L \approx 2.4$.

- The "starfish torus" has a surface Γ of genus 1, with generating curve

$$r(s) = 1 + 0.5(1 + 0.25\sin(5s))(\cos(s), \sin(s)), \qquad s \in [-\pi, \pi], \tag{71}$$

  and generalized diameter $L \approx 3.2$.

The incident fields, when such are present, are either (44) or (47). These are all of order 1 on Γ, except H^0 in (47), which is of order $|k_- \log(k_-)|$.

Our computations rely on Fourier–Nyström discretization [32], where a sequence of decoupled modal problems, with modal index n, are solved using a mix of 16th- and 32nd-order composite panel-based discretization and where linear systems are solved iteratively using GMRES with a

stopping criterion threshold of machine epsilon in the estimated relative residual. The implementation of this numerical scheme is the same as that used in [17, Sec. 10]. In particular, the scheme is thoroughly verified for Dirac (A) and genus 0 in [17, Sec. 10.3] both under mesh refinement and by comparison with semi-analytic results. In the present work, Dirac (A∞-aug) and (B-aug0/1) are verified against Dirac (A) to the extent possible. The codes are implemented in MATLAB, release 2020a, and executed on a workstation equipped with an Intel Core i7-3930K CPU and 64 GB of RAM.

Both fields (44) and (47) are axially symmetric and excite only the mode $n = 0$, which is the only Fourier mode affected by our augmentations for any incident field. More precisely, in all our augmentations bc for Dirac (A∞-aug) and (B-aug0/1), the vector b is a mode-0 function, whereas $ch = 0$ for all mode-n functions h with $n \neq 0$. This is straightforward to verify, given the fact that $E_k^\pm h$ is a mode-n function, whenever h is such a function. To see the latter, assume that $h_\alpha = e^{in\alpha}h$, where h_α denotes the function h rotated an angle α around the z-axis. Write $h = h^+ + h^-$ in the splitting in Hardy subspaces from [26, Thm. 9.3.9], where $h^\pm = E_k^\pm h$. Denote by $h_\alpha^\pm$ the function $h^\pm$ rotated as above. We have

$$h_\alpha^+ + h_\alpha^- = h_\alpha = e^{in\alpha}h = e^{in\alpha}h^+ + e^{in\alpha}h^-. \tag{72}$$

By the uniqueness in this splitting and the rotational invariance of $\mathbf{D}F = ikF$ and the Dirac radiation condition, it follows that we must have $h_\alpha^\pm = e^{in\alpha}h^\pm$. Thus $E_k^\pm h = h^\pm$ are also mode-n functions as claimed.

Several of our experiments result in field images and error images. When assessing the accuracy of computed fields, and in the absence of semi-analytic results, we adopt a procedure where to each numerical solution we also compute an overresolved reference solution, using roughly 50% more points in the discretization of the system under study. The absolute difference between these two solutions is denoted the *estimated absolute error*. The fields are always computed at 90,000 field points on a Cartesian grid in the computational domains shown.

8.1. The number of accurate digits in field evaluations

Since the transmitted and scattered fields differ much in size, it is important to measure their relative errors appropriately. In the exterior Ω_-, the measurable fields are $E^0 + E^-$ and $H^0 + H^-$. Hence it is motivated to normalize the error in E^- and H^- by the maximum of $|E^0 + E^-|$ and $|H^0 + H^-|$ in Ω_-, respectively. In the interior Ω_+, the measurable fields are E^+ and H^+. Hence it is motivated to normalize the error in E^+ and H^+ by the maximum of $|E^+|$ and $|H^+|$ in Ω_+. However, note that when $k_\pm \approx 0$, all field components are almost harmonic functions and the maximum principle for such functions motivates replacing the above maxima by the maxima of each field component on Γ. Summarizing, we use the relative errors

$$\left\{ \frac{\max_{\Omega_+} |E_{\text{err}}^+|}{\max_\Gamma |E^+|}, \frac{\max_{\Omega_- \cap \mathcal{D}} |E_{\text{err}}^-|}{\max_\Gamma |E^0 + E^-|}, \frac{\max_{\Omega_+} |H_{\text{err}}^+|}{\max_\Gamma |H^+|}, \frac{\max_{\Omega_- \cap \mathcal{D}} |H_{\text{err}}^-|}{\max_\Gamma |H^0 + H^-|} \right\} \tag{73}$$

in the four fields $\{E^+, E^-, H^+, H^-\}$, where $\mathcal{D}$ denotes the computational domain and F_{err} denotes the estimated absolute error in a field F. The *number of accurate digits* in a field F is

$$Y = -\text{round}(\log_{10} \epsilon), \tag{74}$$

where ϵ denotes the relative error defined in (73).

Note that the relative error in the equally measurable eddy current J, will be the same as the relative error in E^+.

8.2. The high conductivity "rotated starfish"

We consider the field (44) incident on the "rotated starfish" with $L \approx 2.4$ cm defined by (70), at wavenumbers $k_- = 10^{-8}$ cm^{-1} and $k_+ = 1 + i$ cm^{-1}. This corresponds to a frequency $\omega \approx 300$ rad/s and conductivity $\sigma \approx 5.3 \cdot 10^7$ S/m, which for example occurs for copper. Since the surface Γ has genus 0, we compute the scattered and transmitted fields using Dirac (B-aug0). The number of accurate digits (74) obtained for the fields $\{E^+, E^-, H^+, H^-\}$ are $\{13, 14, 13, 14\}$ and GMRES needs 33 iterations. The amplitudes of a selection of components of the fields $E^\pm$ and $H^\pm$ are
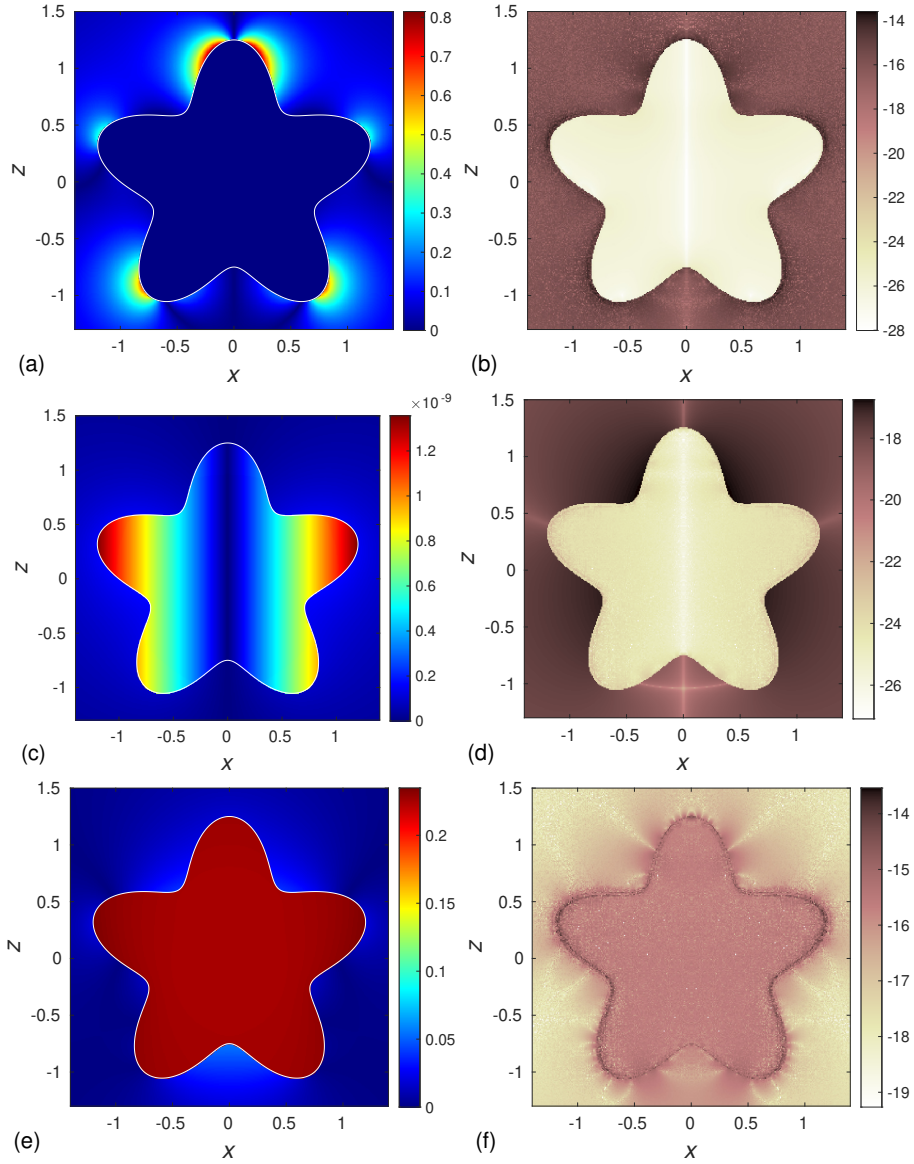
Figure 3: Field images for scattering of (44) by the "rotated starfish" (70) at $k_- = 10^{-8}, k_+ = 1 + i$; (a) scattered/transmitted amplitude $|E_\rho|$; (c) scattered/transmitted amplitude $|E_\theta|$; (e) scattered/transmitted amplitude $|H_z|$. (b,d,f) $\log_{10}$ of estimated absolute error of complex fields using (B-aug0), for (a,c,e) respectively.

shown in Figure 3 along with field errors. Note that, unlike (74), the errors shown in Figures 3–6 are estimated absolute errors. The component E_z is similar to E_ρ and shows a scattered electric field E^- which is close to normal on Γ. Figure 3(c) shows that the transmitted electric field E^+ is of order 10^{-9}. Figure 3(e) shows that most of the incident magnetic field H^0, which is mainly in the z direction, is transmitted into the non-magnetic object. The components H_ρ and H_θ (not shown) are of order 10^{-2} and 10^{-9} respectively. This agrees with the discussion beginning Section 5 which predicts all the fields to be of order 1 except E^+, which is of order $k_- = 10^{-8}$ cm^{-1}.

For comparison, solving the same scattering problem with Dirac (A∞-aug) takes 36 iterations and gives $\{5, 14, 6, 6\}$ accurate digits for $\{E^+, E^-, H^+, H^-\}$. This gives numerical support for choosing (B-aug0) for eddy current scattering with surfaces of genus 0. This is so since (A∞-aug) computes the fields at the wrong scale (50), with subsequent loss of accuracy.

8.3. The high conductivity "starfish torus"

We consider the "starfish torus" with $L \approx 3.2$ cm defined by (71), again at wavenumbers $k_- = 10^{-8}$ cm^{-1} and $k_+ = 1 + i$ cm^{-1}.
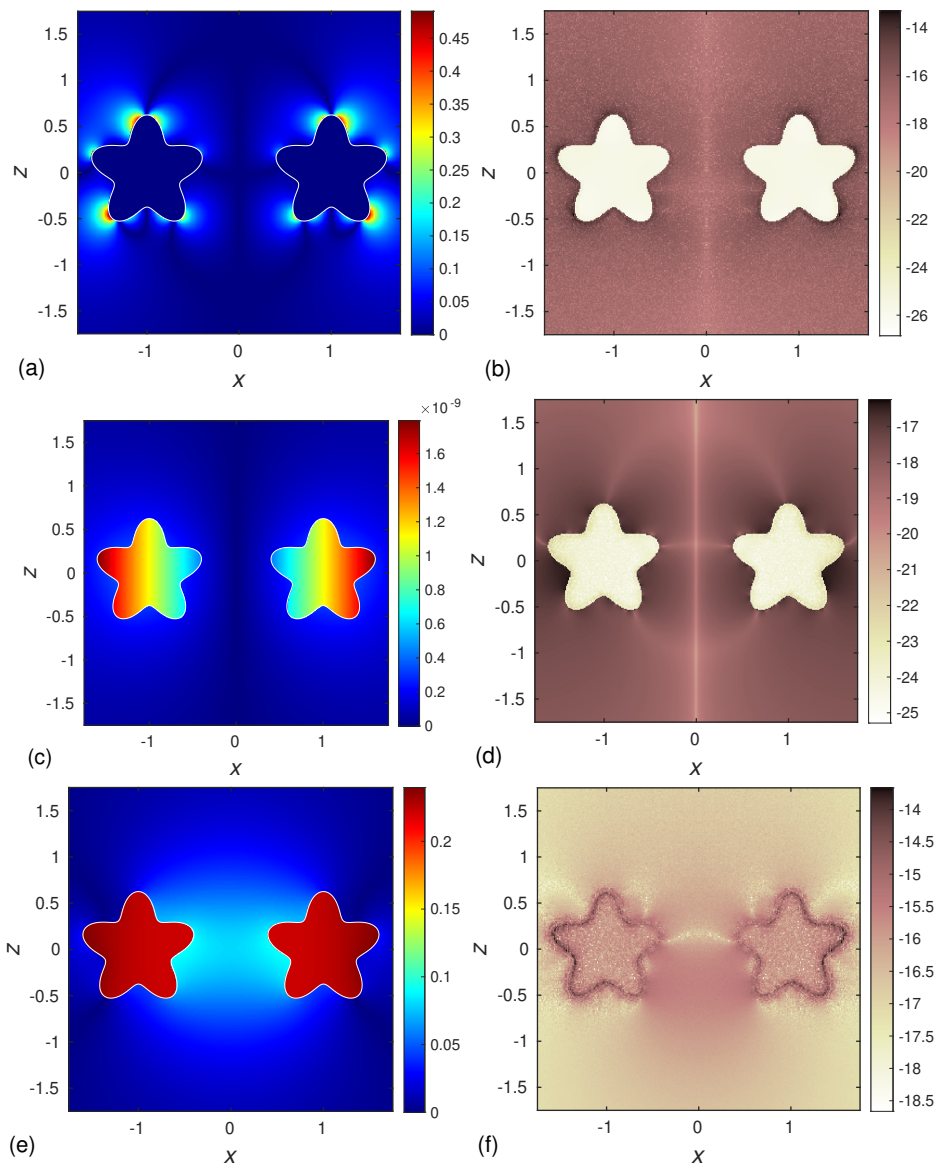
Figure 4: Field images for scattering of (44) by the "starfish torus" (71) at $k_- = 10^{-8}, k_+ = 1 + i$; (a) scattered/transmitted amplitude $|E_\rho|$; (c) scattered/transmitted amplitude $|E_\theta|$; (e) scattered/transmitted amplitude $|H_z|$. (b,d,f) $\log_{10}$ of estimated absolute error of complex fields using (B-aug1), for (a,c,e) respectively.

First, we use the incident field (44), for which $|d_N^1 f^0| / \max_\Gamma |f^0| \approx 0.4$. This indicates that (44) does not excite the Neumann eigenfield and motivates using Dirac (B-aug1). The number of accurate digits obtained for $\{E^+, E^-, H^+, H^-\}$ are $\{13, 13, 13, 14\}$, and GMRES needs 37 iterations. Solving the single block system (68), which is needed only once for a given Γ, requires 20 iterations. The amplitudes of a selection of components of the fields $E^\pm$ and $H^\pm$ are shown in Figure 4 along with field errors. Qualitatively, the result is similar to that in Section 8.2.

For comparison, solving the same scattering problem with Dirac (A∞-aug) also takes 37 iterations but gives $\{6, 13, 7, 7\}$ accurate digits for $\{E^+, E^-, H^+, H^-\}$. This gives numerical support for choosing (B-aug1) for eddy current scattering with surfaces of genus 1 when the Neumann eigenfield is not excited. This is so since (A∞-aug) computes the fields at the wrong scale (50), with subsequent loss of accuracy.

Second, we use the incident field (47), for which $|d_N^1 f^0| / \max_\Gamma |f^0| \approx 6 \cdot 10^7$. This indicates that (47) does excite the Neumann eigenfield, and motivates using Dirac (A∞-aug). The number of accurate digits obtained for $\{E^+, E^-, H^+, H^-\}$ are $\{13, 14, 13, 13\}$ and GMRES needs 24 iterations. The amplitudes of a selection of components of the fields $E^\pm$ and $H^\pm$ are shown in Figure 5 along
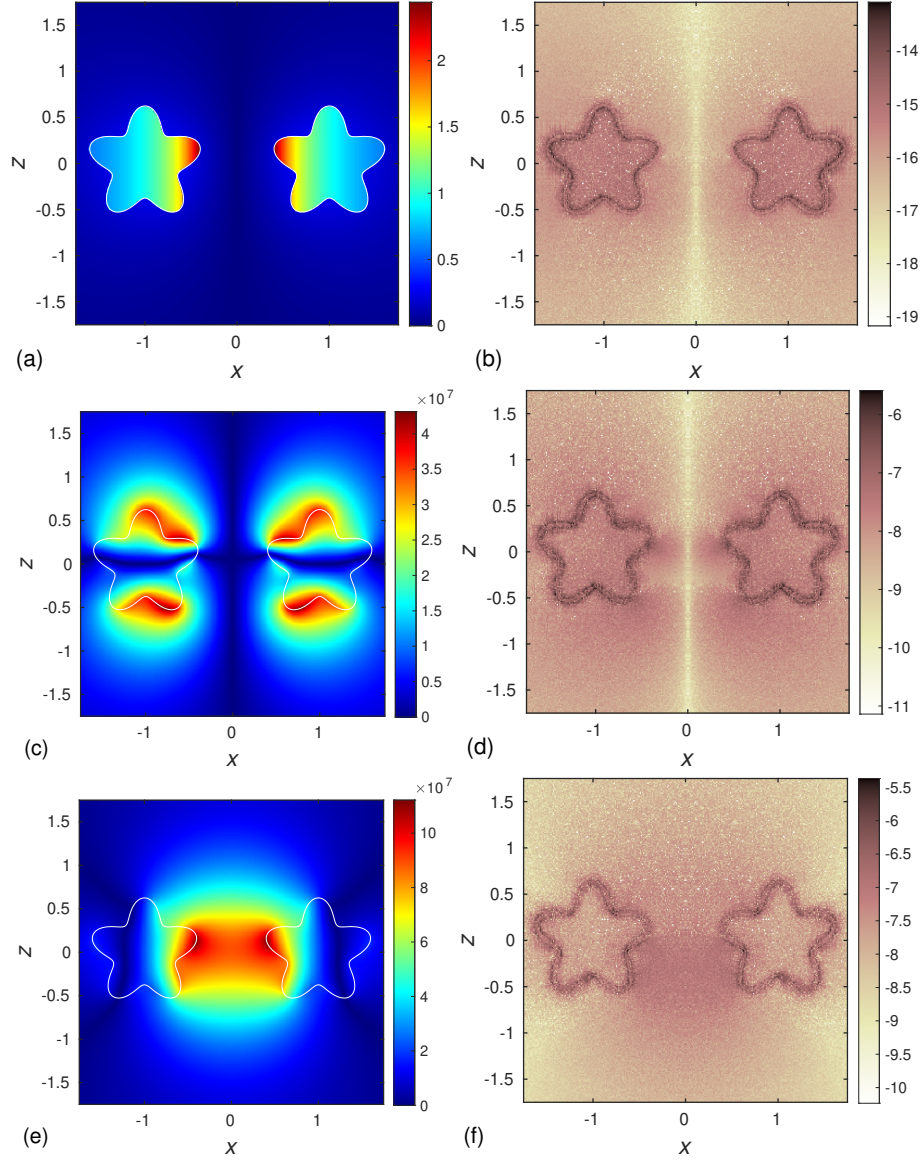
20

Figure 5: Field images for scattering of (47) by the "starfish torus" (71) at $k_- = 10^{-8}, k_+ = 1 + i$; (a) scattered/transmitted amplitude $|E_\theta|$; (c) scattered/transmitted amplitude $|H_\rho|$; (e) scattered/transmitted amplitude $|H_z|$. (b,d,f) $\log_{10}$ of estimated absolute error of complex fields using (A∞-aug), for (a,c,e) respectively.

with field errors. It is clearly seen that the incident field (47) does excite the Neumann field. The scattered and transmitted fields are very similar to those shown in Figure 2(g,h,i), except for the scale. Note that $k_-^{-1}E^+$ and $H^\pm$ are of order 10^8, which is the scale (54) that (A∞-aug) is adapted to, and a factor of 10^8 larger than the scale of a generic field as in the discussion beginning Section 5. The components E_ρ, E_z, and H_θ (not shown) are of order 10^{-16}, 10^{-16}, and 10^{-9}.

For comparison, solving the same scattering problem with Dirac (B-aug1) takes 32 iterations and gives $\{13, 7, 13, 13\}$ accurate digits for $\{E^+, E^-, H^+, H^-\}$. This gives numerical support for choosing (A∞-aug) for eddy current scattering with surfaces of genus 1 when the Neumann eigenfield is excited. To see why (B-aug1) gives loss of accuracy in E^- in this example, note that the right-hand side in (69) is of order 10^8 due to $d_N^1 f^0$ in the second term. Since the system in (69) is well-conditioned and has norm of order 1, the density h will also be of order 10^8. When finally computing the fields with (62) then, according to (54), if no cancellation occurs E^- will be of order 10^8. But as we see in Figure 5(a) E^- is of order 1, and this is due to cancellation in (62) which leads to the loss of accuracy.
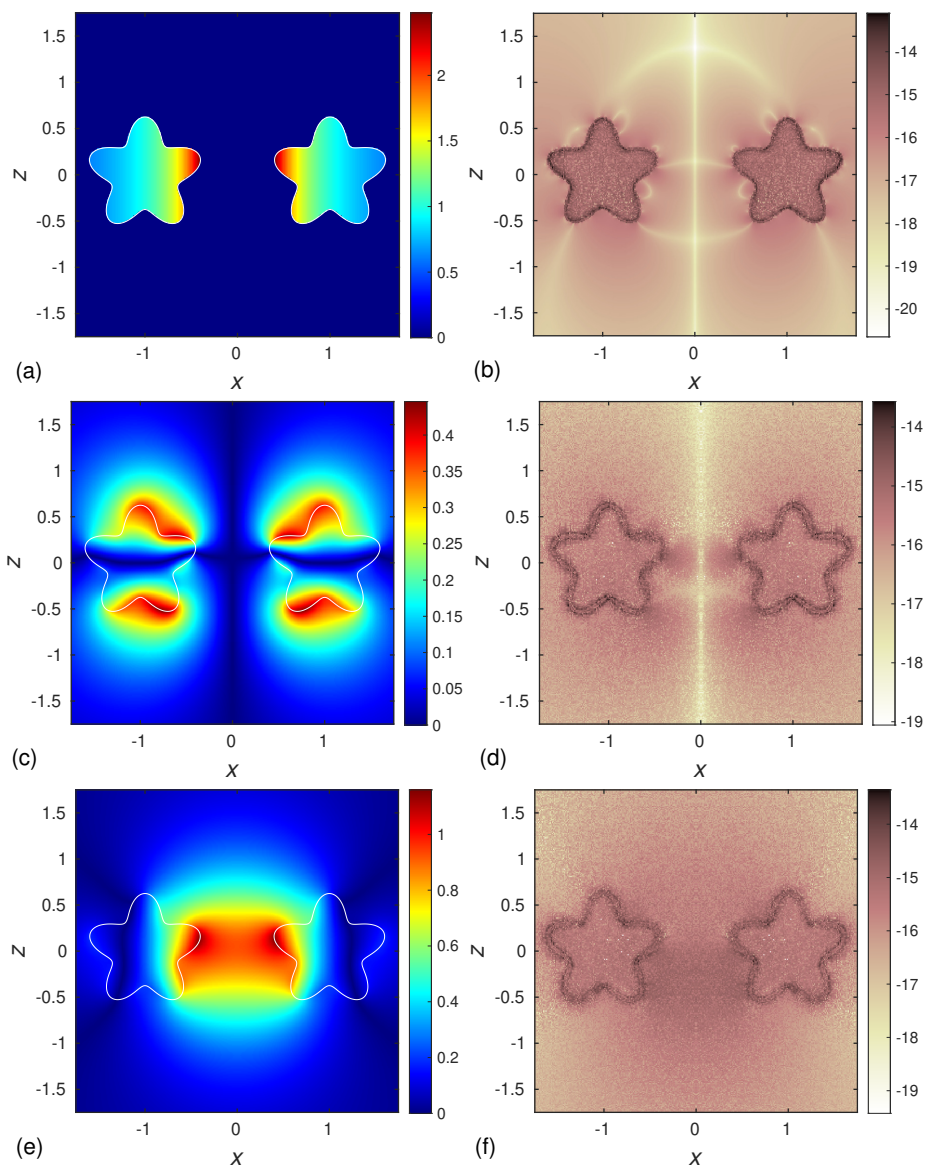
Figure 6: Field images for scattering of (47) by the "starfish torus" (71) at $k_- = 10^{-8}, k_+ = 10^{-4}(1+i)$; (a) scattered/transmitted amplitude $|E_\theta|$; (c) scattered/transmitted amplitude $|H_\rho|$; (e) scattered/transmitted amplitude $|H_z|$. (b,d,f) $\log_{10}$ of estimated absolute error of complex fields using (A∞-aug), for (a,c,e) respectively.

8.4. The medium conductivity "starfish torus"

We consider the field (47) incident on the "starfish torus" (71) with $L \approx 3.2$ cm, now at wavenumbers $k_- = 10^{-8}$ cm^{-1} and $k_+ = 10^{-4}(1+i)$ cm^{-1}. This corresponds to a frequency $\omega \approx 300$ rad/s and a conductivity $\sigma \approx 0.53$ S/m, which for example occurs for seawater. Furthermore, $|d_N^1 f^0|/\max_\Gamma |f^0| \approx 4 \cdot 10^7$, which indicates that (44) does excite the Neumann eigenfield and motivates using Dirac (A∞-aug). The number of accurate digits obtained for $\{E^+, E^-, H^+, H^-\}$ are $\{13, 15, 13, 13\}$ and GMRES needs 16 iterations. The amplitudes of a selection of components of the fields $E^\pm$ and $H^\pm$ are shown in Figure 6 along with field errors. This result is very similar to Figure 5, with the difference that J and H are a factor of 10^8 smaller now. However, since the conductivity is also a factor of 10^8 smaller, the transmitted electric field E^+ has barely changed and the fields E^+ and $H^\pm$ are still a factor of 10^8 larger than what is expected in a generic scattering situation, according to the discussion beginning Section 5. The important point that we want to make is that, although none of the transmitted and scattered fields $E^\pm$, $H^\pm$ are significantly larger than the incident fields E^0, H^0, we are looking at an excited Neumann eigenfield, according to (45). Indeed, in the generic scattering situation when the eigenfield is not excited, the magnitude
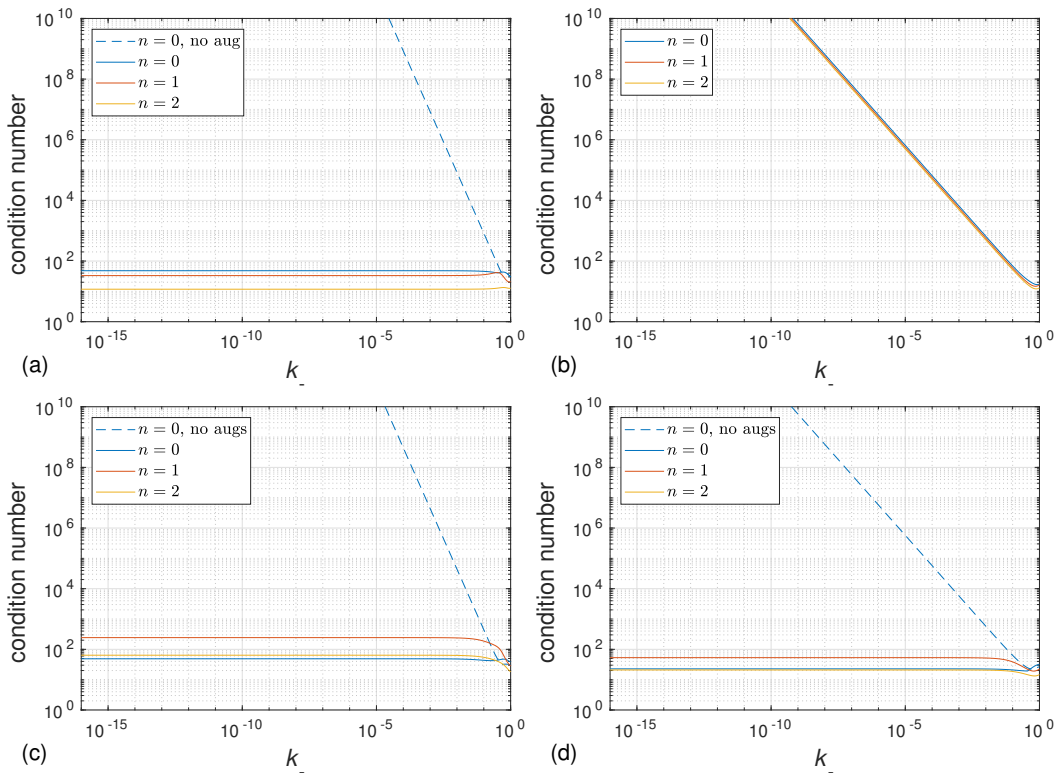
22

Figure 7: The "starfish torus" (71) at high conductivities $k_- \in [10^{-16}, 1]$, $k_+ = 1 + i$. First row: condition numbers for (A∞-aug); (a) system (52); (b) field representation (28). Second row: condition numbers for (B-aug1); (c) system (69); (d) field representation (62).

of E^+ would be of order 10^{-8}.

For comparison, solving the same scattering problem with Dirac (B-aug1) takes 27 iterations and gives $\{13, 8, 13, 13\}$ accurate digits for $\{E^+, E^-, H^+, H^-\}$. Again this gives numerical support for choosing (A∞-aug) for eddy current scattering with surfaces of genus 1 when the Neumann eigenfield is excited.

8.5. Condition numbers for systems and field representations

We here examine Dirac (A∞-aug) and Dirac (B-aug1) from a condition number point of view. Recall from the discussion in the Introduction that the computation of the transmitted and scattered fields involves (a) solving a linear system for the density h, followed by (b) applying the field formulas to h. The important point that we want to stress is that condition numbers for the system (a) alone give insufficient information for assessing a BIE. Indeed, Figure 7(a) shows that Dirac (A∞-aug), after augmentation, has a well-conditioned system. But we have seen that (A∞-aug) in general only computes the fields accurately when the Neumann eigenfield is excited. Figure 7(b) reveals that the important missing information is that the field representation (28) is ill-conditioned for (A∞-aug), for all modes n. We see a low-frequency breakdown in this field representation since it fails to be a Fredholm map as $k_- \to 0$. This is unavoidable since the only way that (A∞-aug) can compute fields much smaller than the Neumann eigenfield is by cancellation in the field evaluations. To be precise, the condition numbers in Figure 7(b,d) refer to the map

$$h \mapsto (\hat{k}^2/\langle\sigma\rangle E^+|_\Gamma, E^-|_\Gamma, H^+|_\Gamma, H^-|_\Gamma), \tag{75}$$

where we have scaled the fields by their generic size in the eddy current regime, as discussed in Section 5.

Figure 7(c,d) shows that for (B-aug1), we have succeeded in constructing a BIE where both the system and the field representation are well-conditioned, after augmentation. That this is possible for (B-aug0) and genus 0 is perhaps less surprising, since the MTP in this case is well-conditioned.
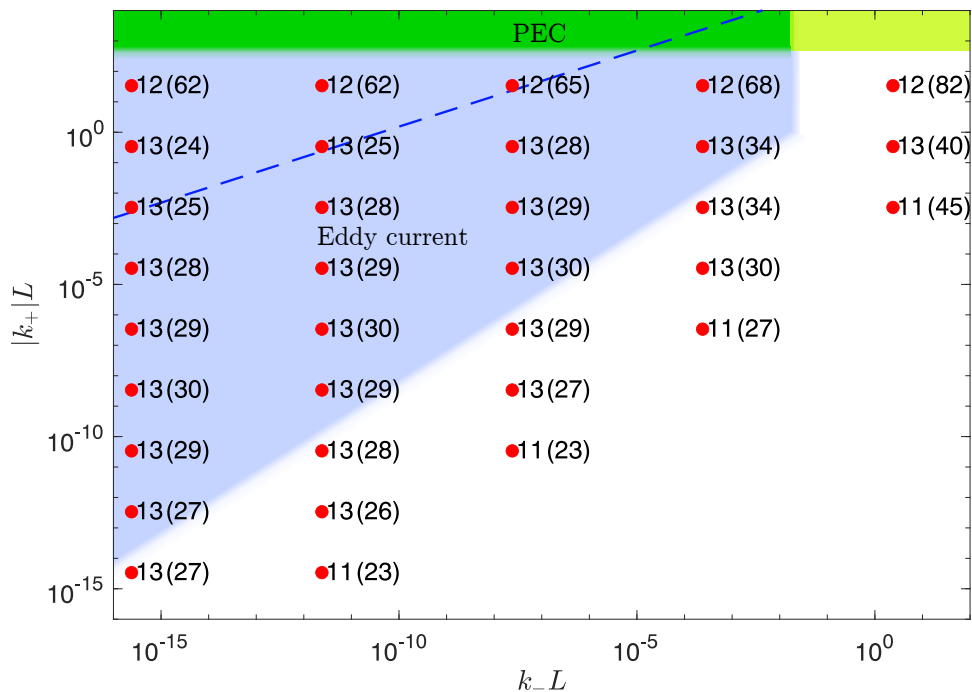
23

Figure 8: Performance in the eddy current regime of Dirac (B-aug0) on the "rotated starfish" (70) with incident partial waves (44). Notation as in Figure 1.

But for (B-aug1) and genus 1, we recall that the MTP itself is ill-conditioned. Our design of (B-aug1) is such that the Neumann eigenfield is hiding in the preprocessing, the computation of the right-hand side in (69), and in particular in computing $d_N^1 f^0$. To be precise, in order to assess the efficiency of a BIE one must take into account three computations: the preprocessing involved in computing the right-hand side g in (5), the solution of the main linear system that produces the density h, and finally the postprocessing involved in computing the fields $F^\pm$. For our ill-conditioned MTP, it is clearly the best option to let the Neumann eigenfield appear only in the preprocessing, as in (B-aug1). It should be noted that $d_N^1 f^0$ in general requires careful computation, since for general incident fields f^0 this integral involves cancellations. However, for mode-0 fields like (44) and (47) there are no such cancellations.

8.6. Performance of (B-aug0/1) in the eddy current regime

We conclude this section by surveying the accuracy and speed of Dirac (B-aug0/1) across the regime (4), with the incident field (44), which we have seen does not excite the Neumann eigenfield. We compute the minimum number of accurate digits, as defined in Section 8.1, in the four fields $\{E^+, E^-, H^+, H^-\}$ at all 90,000 field points in the computational domain. This minimum Y, at pairs of wavenumbers across the regime (4), is reported in Figure 1 for Dirac (B-aug1) and the "starfish torus" (71), and in Figure 8 for Dirac (B-aug0) and the "rotated starfish" (70). Within parentheses is also reported in these figures, the number of iterations X that it takes GMRES to compute the density h. We conclude that there is no low-frequency breakdown for Dirac (B-aug0/1) in the regime (4).

As customary, we also show, in Figure 9, results analogous to those in Figure 8 but for the unit sphere and where the reference solutions are semi-analytic solutions given by Mie theory – rather than overresolved, purely numerical, solutions. The computational domain is $\mathcal{D} = \{-2 \leq x \leq 2, -2 \leq z \leq 2\}$. Figure 9 shows that the solutions obtained with Dirac (B-aug0) in the eddy current regime agree with the Mie solutions at least as well as they agree with the overresolved reference solutions in Figure 8. The number of GMRES iterations required is lower, however, because the scattering problem on the sphere is simpler.
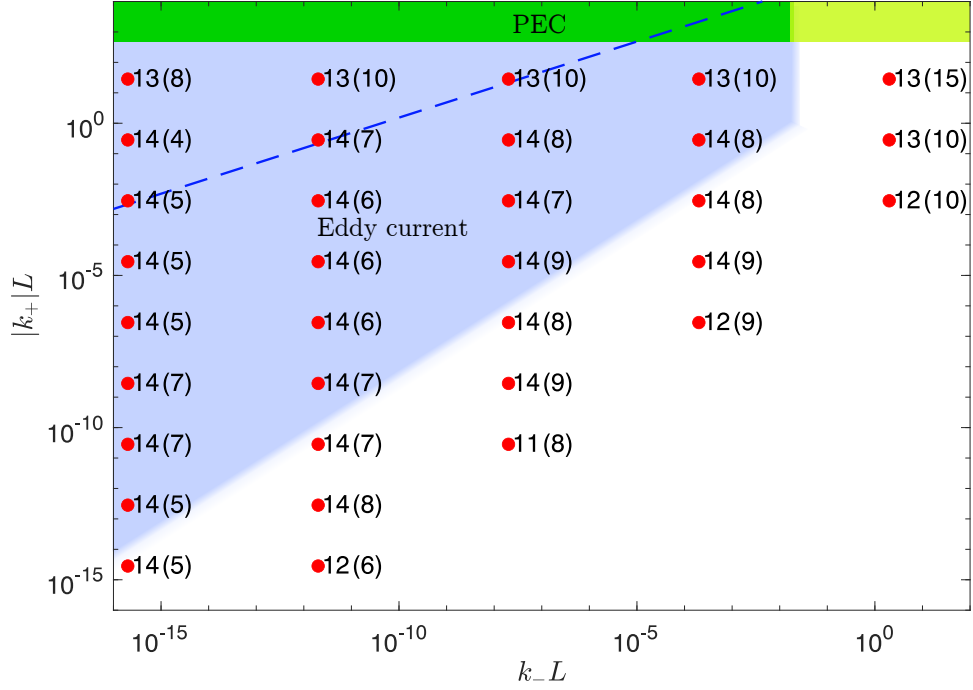
Figure 9: Performance in the eddy current regime of Dirac (B-aug0) on the unit sphere with incident partial waves (44) and with reference solutions from Mie theory. Notation as in Figure 1.

9. The Maxwell essential spectrum

We prove in this section the following result, announced in [17, Sec. 6].

Theorem 1. *Let* $\Gamma \subset \mathbf{R}^3$ *be a bounded Lipschitz surface, and let* $k_\pm \in \mathbf{C} \setminus \{0\}$, $\mathrm{Im}\,(k_\pm) \geq 0$. *Assume that* $\hat{k}$ *is not negative real. Then the non-magnetic Maxwell transmission problem* $MTP(k_-,k_+,\hat{k}^2)$ *defines a Fredholm map, in* L^2_{loc} *norm of the fields up to* Γ, *if and only if*

$$(1 + \hat{k}^2)/(1 - \hat{k}^2) \notin \sigma_{ess}(K_0^{\nu'}; H^{1/2}(\Gamma)), \tag{76}$$

where $K_0^{\nu'}$ *is the Neumann–Poincaré operator, that is (17) with* $k = 0$.

Note that for all passive non-magnetic materials, the technical condition that $\hat{k}$ should not be negative real, is always satisfied. The essential spectrum appears when $\hat{\epsilon} = \hat{k}^2$ is negative real. In three dimensions, $\sigma_{ess}(K_0^{\nu'}; H^{1/2}(\Gamma))$ may be non-symmetric with respect to 0. Theorem 1 shows in particular that the Fredholm property of $MTP(k_-,k_+,\hat{k}^2)$ only depends on $\hat{\epsilon}$, and is not in general symmetric when replacing $\hat{\epsilon}$ by $\hat{\epsilon}^{-1}$.

PROOF. The idea is to use an auxiliary Dirac BIE with parameters

$$\begin{bmatrix} r & \beta & \gamma & \alpha' & \beta' & \gamma' \end{bmatrix} = \begin{bmatrix} 1/\hat{k} & 1 & 1 & 1/\hat{k} & 1/\hat{k} & 1 \end{bmatrix}. \tag{77}$$

Here we are not concerned with false eigenwavenumbers, and have tuned the free Dirac parameters only so that we avoid false essential spectrum, assuming that $\hat{k}$ is not negative real. Preconditioning is also irrelevant for this proof, and we let $P = P' = I$. Consider the Dirac integral operator

$$E_{k_+}^+(rM') + ME_{k_-}^- = \tfrac{1}{2}(rM' + M + E_{k_+}(rM') - ME_{k_-}) \tag{78}$$

from (22). With our choice of parameters (77), we have

$$rM' + M = \mathrm{diag}\begin{bmatrix} 1 + \tfrac{1}{\hat{k}} & \tfrac{1}{\hat{k}} + \tfrac{1}{\hat{k}} & \tfrac{1}{\hat{k}} + \tfrac{1}{\hat{k}} & 1 + 1 & 1 + \tfrac{1}{\hat{k}^2} & \tfrac{1}{\hat{k}} + 1 \end{bmatrix}. \tag{79}$$

Modulo compact operators, the operator $E_{k_+}(rM') - ME_{k_-}$ equals the entry-wise product of

$$
\begin{bmatrix}
1-\frac{1}{\hat k} & 0 & \mathbf{\frac{1}{\hat k}-\frac{1}{\hat k}} & 0 & \hat k-\frac{1}{\hat k} & \mathbf{0} \\
1-\frac{1}{\hat k} & \frac{1}{\hat k}-\frac{1}{\hat k} & \mathbf{\frac{1}{\hat k}-\frac{1}{\hat k}} & \hat k-\frac{1}{\hat k} & 0 & 1-\frac{1}{\hat k} \\
\mathbf{1}-\frac{1}{\hat k} & \frac{1}{\hat k}-\frac{1}{\hat k} & \frac{1}{\hat k}-\frac{1}{\hat k} & \mathbf{\hat k}-\frac{1}{\hat k} & 0 & 1-\frac{1}{\hat k} \\
0 & 1-1 & \mathbf{0} & 1-1 & 0 & \frac{1}{\hat k}-1 \\
\hat k-\frac{1}{\hat k^2} & 0 & \mathbf{1}-\frac{1}{\hat k^2} & 1-\frac{1}{\hat k^2} & 1-\frac{1}{\hat k^2} & \frac{1}{\hat k}-\frac{1}{\hat k^2} \\
\mathbf{\hat k-1} & \mathbf{0} & \mathbf{1-1} & \mathbf{1-1} & \mathbf{1-1} & \frac{1}{\hat k}-1
\end{bmatrix}
\tag{80}
$$

(not simplifying some entries to zero in order to show what cancellations occur) and E_k from (15), with Φ_k replaced by Φ_0 in the operators, and the factor ik_- in front of the single layer operators. See [18, Eq. (132)]. The compactness of the approximation of E_k was proved in [2, Lem. 3.20].

We now exploit a number of block triangular structures, modulo compact operators, in the matrix (78) which (77) entails. Recall from [18, Sec. 5] that the Dirac integral operator acts in the function space

$$
\mathcal{H}_3 = H^{1/2}(\Gamma) \oplus H^{-1/2}(\Gamma) \oplus H^{-1/2}(\mathrm{curl},\Gamma) \oplus H^{1/2}(\Gamma) \oplus H^{-1/2}(\Gamma) \oplus H^{-1/2}(\mathrm{curl},\Gamma), \tag{81}
$$

which coincides, up to equivalence of norms, with the function space $\mathcal{E}$ from [2]. Note that we here have omitted the Hodge star present in [18, Eq. (64)], since we in the present paper conform to the standard vector representation of the magnetic field. The function space $H^{-1/2}(\mathrm{curl},\Gamma)$ consists, roughly speaking, of tangential vector fields in $H^{-1/2}$ with tangential curl also in $H^{-1/2}$. The precise definition of $H^{-1/2}(\mathrm{curl},\Gamma)$ on Lipschitz Γ is in [18, Eq. (65)].

First, we claim that the (5:8,1:4) block is compact. Indeed, the only possibly non-compact operators are in blocks (5,2) and (7:8,3:4), and here we have cancellation $1-1$. This shows that (78) is a Fredholm operator on $\mathcal{H}_3$ if and only if its diagonal (1:4,1:4) and (5:8,5:8) blocks are so. Second, within these diagonal blocks we have cancellation in blocks (1:2,3:4) and (7:8,5:6). This gives a block triangular structure inside the diagonal (1:4,1:4) and (5:8,5:8) blocks, which shows that (78) is Fredholm if and only if its diagonal (1,1), (2,2), (3:4,3:4), (5,5), (6,6) and (7:8,7:8) blocks are Fredholm operators. This is true for the (2,2), (3:4,3:4) and (5,5) blocks, since these operators are $(1/\hat k)I_{H^{-1/2}(\Gamma)}$, $(1/\hat k)I_{H^{-1/2}(\mathrm{curl},\Gamma)}$ and $I_{H^{1/2}(\Gamma)}$, respectively. Also the (1,1) and (7:8,7:8) blocks in (78) are Fredholm operators since by assumption $(\hat k+1)/(\hat k-1) \notin (-1,1)$, and the essential spectra of $K_0^{\nu'} : H^{1/2}(\Gamma) \to H^{1/2}(\Gamma)$ and $\boldsymbol{M}_k^* : H^{-1/2}(\mathrm{curl},\Gamma) \to H^{-1/2}(\mathrm{curl},\Gamma)$ are contained in $(-1,1)$. This is a well-known consequence of the Plemelj symmetrization principle and boundary Hodge decompositions. A precise reference is [2, Cor. 4.7(i)], which contains the spectral estimates of both $K_0^{\nu'}$ and $\boldsymbol{M}_0^*$ upon letting $k=0$ and writing E_k in matrix form as in (15).

We conclude that (78) is a Fredholm operator if and only if the (6,6) block is so, which by duality is equivalent to (76). Moreover, assuming that $\hat k$ is not negative real, then the auxiliary Maxwell and Helmholtz problems corresponding to the parameters $\beta, \gamma, \alpha', \beta', \gamma'$, all define Fredholm maps, and it follows from the proofs of [18, Props. 8.4, 8.5] that (78) is a Fredholm operator if and only if $\mathrm{MTP}(k_-, k_+, \hat k^2)$ defines a Fredholm map. Combining these two equivalences completes the proof.

10. Concluding remarks

We conclude with some guiding remarks for the reader chiefly interested in coding the BIEs proposed in this paper. Eddy current computations are difficult since it is difficult to achieve both (a) a well-conditioned BIE for computing the density h and (b) a well-conditioned representation of the fields. Dirac (B-aug0), presented in Section 7.1, always achieves (a) and (b) for boundary surfaces of genus 0. Dirac (B-aug1), presented in Section 7.2, almost always achieves (a) and (b) for boundary surfaces of genus 1. There are no null spaces for the systems and there are no low-frequency breakdowns in these two integral equation reformulations for the Maxwell transmission problem. The only incident field which leads to loss of accuracy with Dirac (B-aug1) for genus 1 is (47), which is a pathological field which typically does not appear in applications. For (47) we can accurately compute the fields with Dirac (A∞-aug), as presented in Section 6.1.

Appendix A. Augmentations

In this appendix, we derive the augmentations proposed in Sections 6 and 7, following the general principles explained in Section 4. Throughout this section, we consider the limit as $k_- \to 0$ in the eddy current regime (4). To be able to perform the analysis below, we set the tuning factor $\xi = 1$, and also assume that $k_+ \to 0$. Note that this holds for all ordinary conductors. For nonphysical limits when $\sigma \to \infty$ so that $k_+ \not\to 0$, the analysis below needs to be adjusted and becomes more complicated. However, the heuristics is that the larger $|k_+|$ is, the fewer augmentations are needed. We denote by K and S, operators of the form

$$Kf(x) = \text{p.v.} \int_\Gamma v(x,y) \cdot \nabla \Phi_0(y-x) f(y) d\Gamma(y), \qquad x \in \Gamma, \tag{A.1}$$

and

$$Sf(x) = k_+ \hat{k}/\langle \sigma \rangle \int_\Gamma u(x,y) \Phi_0(y-x) f(y) d\Gamma(y), \qquad x \in \Gamma, \tag{A.2}$$

for some given vector fields $v(x,y)$ and scalar functions $u(x,y)$. Note that $|k_+ \hat{k}/\langle \sigma \rangle| \leq 1$.

We recall that $\mathsf{N}(I + K_0^{\nu'})$ is spanned by the constant function 1, that $(K_0^{\nu'})^* = -K_0^\nu$, and that $\mathsf{N}(I - K_0^\nu)$ is spanned by $f = N_{\Omega_-}(1)$, where N_{Ω_-} is the Dirichlet-to-Neumann map for Ω_-. Further recall that the spectrum of all operators $K_0^{\nu'}, K_0^\nu$ and $\boldsymbol{M}_0^*$ are contained in $[-1,1]$, with $\sigma(K_0^{\nu'}) \cap \{-1,+1\} = \{-1\}$ and $\sigma(K_0^\nu) \cap \{-1,+1\} = \{+1\}$. Further $\sigma(\boldsymbol{M}_0^*) \cap \{-1,+1\} = \emptyset$ if the genus of Γ is zero and otherwise equals $\{-1,+1\}$.

Dirac (A∞-aug)

The limit of $I + G$ is seen to be

$$I + G_0^A = \begin{bmatrix} I - K_0^{\nu'} & 0 & \boldsymbol{0} & 0 & S & \boldsymbol{0} \\ K & I - \frac{a-1}{a+1} K_0^\nu & \boldsymbol{0} & S & 0 & \boldsymbol{S} \\ \boldsymbol{K} & \boldsymbol{K} & \boldsymbol{I} & \boldsymbol{S} & 0 & \boldsymbol{S} \\ 0 & 0 & \boldsymbol{0} & I - \frac{a-1}{a+1} K_0^{\nu'} & 0 & \boldsymbol{0} \\ 0 & 0 & \boldsymbol{0} & K & I - K_0^\nu & \boldsymbol{K} \\ \boldsymbol{0} & \boldsymbol{0} & \boldsymbol{0} & \boldsymbol{0} & 0 & \boldsymbol{I} + \frac{a-1}{a+1} \boldsymbol{M}_0^* \end{bmatrix}, \tag{A.3}$$

where we assume that $\hat{k} \notin (0,\infty)$ so that $(a-1)/(a+1) \notin [-1,1]$, where $a = \hat{k}/|\hat{k}|$. We note the block triangular structures and that the only non-invertible diagonal block is the (6,6) block. The null space is seen to be spanned by a density of the form $h_D^A = \begin{bmatrix} h_1 & h_2 & \boldsymbol{h_{3:4}} & 0 & f & \boldsymbol{0} \end{bmatrix}$, and we have $c_D^1 h_D^A \neq 0$ at $k_- = 0$. Moreover, the adjoint $(I + G_0^A)^*$ is seen to have null space spanned by a density of the form $\begin{bmatrix} 0 & 0 & \boldsymbol{0} & h_5 & 1 & \boldsymbol{h_{7:8}} \end{bmatrix}$, which is not orthogonal to b_D^1. Therefore the homogeneous (L) augmentation $b_D^1 c_D^1$ will remove the Dirichlet eigenfield, since $c_D^1 h = 0$, that is (8), holds for all incident fields under consideration.

Dirac (B-aug0)

The limit of $I + G$ is seen to be

$$I + G_0^B = \begin{bmatrix} I + K_0^{\nu'} & 0 & \boldsymbol{K} & 0 & 0 & \boldsymbol{0} \\ 0 & I & \boldsymbol{0} & 0 & 0 & \boldsymbol{0} \\ \boldsymbol{0} & \boldsymbol{0} & \boldsymbol{I} & 0 & 0 & \boldsymbol{0} \\ 0 & S & \boldsymbol{0} & I - K_0^{\nu'} & 0 & \boldsymbol{0} \\ S & 0 & \boldsymbol{S} & K & I - K_0^\nu & \boldsymbol{0} \\ \boldsymbol{0} & \boldsymbol{0} & \boldsymbol{0} & \boldsymbol{0} & 0 & \boldsymbol{I} + \boldsymbol{M}_0^* \end{bmatrix}. \tag{A.4}$$

In this section, we assume that Γ has genus 0, so that the (7:8, 7:8) block is invertible. We note again block triangular structures, and now the non-invertible diagonal blocks are the (1,1) and (6,6) blocks. If $(I + G_0^B)h = 0$, then $h = \begin{bmatrix} c1 & 0 & \boldsymbol{0} & 0 & h_6 & \boldsymbol{0} \end{bmatrix}$, where $c \in \mathbf{C}$. Here h_6 satisfies $cS1 + (I - K_0^\nu)h_6 = 0$, which forces $c = 0$ and $h_6 = f$ unless $\int_\Gamma S1d\Gamma$ is zero. Inspection of the operator S appearing in the (6,1) block shows that $\int_\Gamma S1d\Gamma = 2ik_+ \hat{k}/\langle \sigma \rangle |\Omega_+|$, where $|\Omega_+|$

denotes the volume of Ω_+. Therefore the null space includes $h_D = \begin{bmatrix} 0 & 0 & \mathbf{0} & 0 & f & \mathbf{0} \end{bmatrix}$ and, as $k_+\hat{k} \to 0$, also $h_H = \begin{bmatrix} 1 & 0 & \mathbf{0} & 0 & 0 & \mathbf{0} \end{bmatrix}$. A similar argument applied to the adjoint $(I + G_0^B)^*$ shows that its null space always includes $h_D^* = \begin{bmatrix} 1 & 0 & \boldsymbol{h_{3:4}} & 0 & 0 & \mathbf{0} \end{bmatrix}$, but as $k_+\hat{k} \to 0$, also $h_H^* = \begin{bmatrix} 0 & h_2 & \boldsymbol{h_{3:4}} & h_5 & f & \mathbf{0} \end{bmatrix}$.

(1) The homogeneous (L) augmentation $b_H^1 c_H^1$ will remove the additional null space appearing as $k_+\hat{k} \to 0$ since b_H^1 is not orthogonal to h_H^* and since $c_H^1(h_H) \neq 0$. Note that $F_0 = 0$ for any electromagnetic field F satisfying (10), and consequently $c_H^1(h) = 0$ holds for all incident fields under consideration.

(2) The augmentation for h_D is less straightforward since the (6,6) entry in P' vanishes for Dirac (B) at $k_- = 0$, causing the corresponding fields to vanish. This means that the field representation (28) needs to be augmented. Recalling (22), we factorize

$$I + G^B = \begin{bmatrix} PE_{k_+}^+ D^{-1} & -NE_{k_-}^- \end{bmatrix} \begin{bmatrix} DE_{k_+}^+ N' \\ -E_{k_-}^- P' \end{bmatrix} = L^B R^B. \tag{A.5}$$

Taking into account (75) and Remark 1, we have rescaled the interior fields using the size 8×8 matrix $D = \mathrm{diag} \begin{bmatrix} \hat{k} & \hat{k} & \boldsymbol{\hat{k}} & \hat{k}^2/\langle\sigma\rangle & \hat{k}^2/\langle\sigma\rangle & \boldsymbol{\hat{k}^2/\langle\sigma\rangle} \end{bmatrix}$. In what follows, we write $\widetilde{E}^\pm = \frac{1}{2}(I \pm \widetilde{E})$, where $\widetilde{E}$ denotes the (1:4,1:4) = the (5:8,5:8) block in E_0, and $\widetilde{S}$ denotes the (5:8,1:4) block in E_0, but with ik replaced by $ik_+\hat{k}/\langle\sigma\rangle$ in all operators S. For the right factor R^B, corresponding to the field representation, we have

$$DE_{k_+}^+ N' \to \begin{bmatrix} \widetilde{E}^+ & 0 \\ \widetilde{S} & \widetilde{E}^+ D_1 \end{bmatrix} \quad \text{and} \quad E_{k_-}^- P' \to \begin{bmatrix} \widetilde{E}^- & 0 \\ 0 & \widetilde{E}^- D_2 \end{bmatrix}, \tag{A.6}$$

with size 4×4 matrices $D_1 = \mathrm{diag} \begin{bmatrix} 1 & 1 & \boldsymbol{\langle\sigma\rangle^{-1}} \end{bmatrix}$ and $D_2 = \mathrm{diag} \begin{bmatrix} 0 & 0 & \mathbf{1} \end{bmatrix}$. For the left factor L^B, corresponding to the DTP, we have

$$PE_{k_+}^+ D^{-1} \to \begin{bmatrix} D_3\widetilde{E}^+ & 0 \\ S & D_4\widetilde{E}^+ \end{bmatrix} \quad \text{and} \quad NE_{k_-}^- \to \begin{bmatrix} D_5\widetilde{E}^- & 0 \\ 0 & D_6\widetilde{E}^- \end{bmatrix}, \tag{A.7}$$

with size 4×4 matrices $D_3 = \mathrm{diag} \begin{bmatrix} 0 & 1/2 & \boldsymbol{1/2} \end{bmatrix}$, $D_4 = \mathrm{diag} \begin{bmatrix} 1 & 1 & \mathbf{0} \end{bmatrix}$, $D_5 = \mathrm{diag} \begin{bmatrix} 1 & 1/2 & \boldsymbol{1/2} \end{bmatrix}$ and $D_6 = \mathrm{diag} \begin{bmatrix} \langle\sigma\rangle^{-1} & \langle\sigma\rangle^{-1} & \mathbf{1} \end{bmatrix}$.

(3) If h is in the null space for both limit operators in (A.6), then $h_{1:4} = \widetilde{E}^+ h_{1:4} + \widetilde{E}^- h_{1:4} = 0$. From $\widetilde{E}^- D_2 h = 0$ it follows that $h_{7:8}$ is the boundary trace of a harmonic vector field for Ω_+ with tangential boundary conditions. As in [26, Exc. 10.6.12], it follows that $h_{7:8} = 0$, as we assume Γ to have genus 0. Moreover, with $h_{7:8} = 0$, we again see h_D appearing from $\widetilde{E}^+ D_1 h = 0$.

The (R) augmentation $b_D^R c_D^R$ has $c_D^R(h_D) \neq 0$, since $\int_\Gamma f \, d\Gamma \neq 0$. We note that b_D^R appears from applying L^B to the fields $F^+ = 0$ and $F^- = E_{k_-}^- e_6$, and it remains to check that $\widetilde{E}^- e_6$ is not in the range of $\widetilde{E}^- D_2$. This in turn follows from the divergence theorem, since no divergence-free vector field in Ω_+ can have normal component ν.

(4) With the (R) augmented field representation (60), we can now make the homogeneous (L) augmentation $b_D^2 c_D^2$ to remove the Dirichlet eigenfield. As for $b_D^1 c_D^1$, we note that $c_D^2 h = 0$, that is (8), holds for all incident fields under consideration. However, now we use $b_D^2 = e_1$, since this is not orthogonal to h_D^*.

Dirac (B-aug1)

(1) We repeat the augmentations for (B-aug0), but now assume that Γ has genus 1. To be able to perform the analysis, we also assume that $\langle\sigma\rangle \to \infty$. Now $\boldsymbol{I} + \boldsymbol{M}_0^*$ has a one-dimensional null space, leading to additional null vectors h_N and h_N^*, non-zero only in the 7:8 components, for $I + G_0^B$ and $(I + G_0^B)^*$ respectively.

(2) Since the Neumann eigenfield can be excited by sources in Ω_-, we aim to remove the above null space by an inhomogeneous (L) augmentation. For the abstract equation (39), we use

$$(\hat{k}^2/\langle\sigma\rangle)\theta \cdot E^+ - (\hat{k}^2/\langle\sigma\rangle)\theta \cdot E^- = (\hat{k}^2/\langle\sigma\rangle)\theta \cdot E^0, \tag{A.8}$$

which follows by rescaling the first equation in (7). On the left-hand side it is the $\theta \cdot E^+$ term which will be dominant, and the generic size of E^+, as discussed in Section 5, motivates the factor $\hat{k}^2/\langle \sigma \rangle$. However, in computing the fields with (60), we note that the (7:8,7:8) entries in N' vanishes at $k_- = 0$. This indicates that further (R) augmentation is needed for Γ of genus 1.

(3) Inspecting the limit operators in (A.6), we see that the new null vector h_N is the boundary trace of a harmonic vector field in Ω_+ with tangential boundary conditions, and hence h_N is in the θ direction for a torus. Therefore $c_N^R(h_N) \neq 0$ at $k_- = 0$. We note that b_N^R appears from applying L^B to the fields $F^+ = E_{k_+}^+ e_8$ and $F^- = 0$, and it remains to prove that $\widetilde{E}^+ e_8$ is not in the range of $\widetilde{E}^+ D_1$. For this, we assume that e_8 is the boundary trace of the interior Neumann eigenfield, and in particular has zero surface curl. The assumption that $E^+ e_8 = e_8$ is in the range of $\widetilde{E}^+ D_1$ is seen to be equivalent to the existence of a vector field F and a scalar function U in Ω_-, decaying at ∞, with $\nabla \times F = \nabla U$, $\nabla \cdot F = 0$ in Ω_-, and F having tangential part e_8 on Γ. It follows that $G = \nabla \times F$ is an exterior Neumann eigenfield. But since G is a gradient vector field, this forces $G = 0$. It follows that F is curl-free in Ω_-, which contradicts Stokes' Theorem. Therefore e_8 cannot be in the range of $\widetilde{E}^+ D_1$.

(4) With the doubly (R) augmented field representation (62), we adjust the augmentation $b_H^1 c_H^1$ to $b_H^2 c_H^2$, and proceed to the inhomogeneous (L) augmentation $b_N^1 c_N^1$ based on (A.8). We use (62) to write $E^{\pm}$ in terms of h, and integrate (A.8) with respect to $w d\Gamma$. To see that the obtained left-hand side defines a bounded functional $c_N^1 h$ as in (64), we rewrite as follows. That the term $(\hat{k}^2/\langle \sigma \rangle)\theta \cdot E^+$ depends boundedly on h is readily seen by inspecting N'. For the term $(\hat{k}^2/\langle \sigma \rangle)\theta \cdot E^-$, we see from P' that it only depends boundedly on $h_{1:5}$. Inspection of the (8,6) block of E_{k_-} in (15) reveals that this yields a gradient vector field, with zero circulation around the torus. Therefore there is no dependence on h_6 and the Dirichlet (R) augmentation term. Finally we consider the crucial dependence on $h_{7:8}$, which as it stands is unbounded. Note from (15) that the (7:8,7:8) block in $E_{k_-}^-$ is $(\boldsymbol{I} + \boldsymbol{M}_{k_-}^*)/2$. The reason for the specific choice of weight w, is that $w\theta$ is orthogonal to $\mathsf{R}(\boldsymbol{I} + \boldsymbol{M}_0^*)$. This allows us to subtract the zero term $\int_\Gamma ((\boldsymbol{I} + \boldsymbol{M}_0^*)h_{7:8})_8 w d\Gamma/2$ to obtain the third regularized term for $c_N^1 h$ in (64), which depends boundedly on h.

To motivate the choice of b_N^1, we note that $(\boldsymbol{I} + \boldsymbol{M}_0)(h_N^*)_{7:8} = 0$. Hence $h_N^* = \begin{bmatrix} 0 & 0 & \boldsymbol{0} & 0 & 0 & 0 & w \end{bmatrix}$, and it follows that $b_N^1 = e_8$ is not orthogonal to h_N^*.

References

[1] AMMARI, H., BUFFA, A., AND NÉDÉLEC, J.-C. A justification of eddy currents model for the Maxwell equations. *SIAM J. Appl. Math. 60*, 5 (2000), 1805–1823.

[2] AXELSSON, A. Transmission problems for Maxwell's equations with weakly Lipschitz interfaces. *Math. Methods Appl. Sci. 29*, 6 (2006), 665–714.

[3] BONNET, M., AND DEMALDENT, E. The eddy current model as a low-frequency, high-conductivity asymptotic form of the Maxwell transmission problem. *Comput. Math. Appl. 77*, 8 (2019), 2145–2161.

[4] CHHIM, T. L., MERLINI, A., RAHMOUNI, L., GUZMAN, J. E. O., AND ANDRIULLI, F. P. Eddy current modeling in multiply connected regions via a full-wave solver based on the quasi-helmholtz projectors. *IEEE Open Journal of Antennas and Propagation 1* (2020), 534–548.

[5] COLTON, D., AND KRESS, R. *Integral equation methods in scattering theory*, vol. 72 of *Classics in Applied Mathematics*. Society for Industrial and Applied Mathematics (SIAM), Philadelphia, PA, 2013. Reprint of the 1983 original [MR0700400].

[6] COLTON, D., AND KRESS, R. *Inverse acoustic and electromagnetic scattering theory*, vol. 93 of *Applied Mathematical Sciences*. Springer, Cham, [2019] ©2019. Fourth edition of [MR1183732].

[7] COOLS, K., ANDRIULLI, F. P., OLYSLAGER, F., AND MICHIELSSEN, E. Nullspaces of MFIE and Calderón preconditioned EFIE operators applied to toroidal surfaces. *IEEE Trans. Antennas and Propagation 57*, 10, part 2 (2009), 3205–3215.

[8] Egorov, A. V., Kucheryavskiy, S. V., and Polyakov, V. V. Resolution of effects in multi-frequency eddy current data for reliable diagnostics of conductive materials. *Chemometrics and Intelligent Laboratory Systems 160* (2017), 8–12.

[9] Epstein, C. L., Gimbutas, Z., Greengard, L., Klöckner, A., and O'Neil, M. A consistency condition for the vector potential in multiply-connected domains. *IEEE Trans. Magn. 49*, 3 (2013), 1072–1076.

[10] Epstein, C. L., and Greengard, L. Debye sources and the numerical solution of the time harmonic Maxwell equations. *Comm. Pure Appl. Math. 63*, 4 (2010), 413–463.

[11] Epstein, C. L., Greengard, L., and O'Neil, M. Debye sources, Beltrami fields, and a complex structure on Maxwell fields. *Comm. Pure Appl. Math. 68*, 12 (2015), 2237–2280.

[12] Epstein, C. L., Greengard, L., and O'Neil, M. A high-order wideband direct solver for electromagnetic scattering from bodies of revolution. *J. Comput. Phys. 387* (2019), 205–229.

[13] García-Martín, J., Gómez-Gil, J., and Vázquez-Sánchez, E. Non-destructive techniques based on eddy current testing. *Sensors 11*, 3 (2011), 2525–2565.

[14] Greenbaum, A., Greengard, L., and McFadden, G. B. Laplace's equation and the Dirichlet-Neumann map in multiply connected domains. *J. Comput. Phys. 105*, 2 (1993), 267–278.

[15] Guenther, R. B., and Lee, J. W. *Partial differential equations of mathematical physics and integral equations.* Dover Publications, Inc., Mineola, NY, 1996. Corrected reprint of the 1988 original.

[16] Halbritter, J. On surface resistance of superconductors. *Z. Phys. 266*, 3 (1974), 209–217.

[17] Helsing, J., Karlsson, A., and Rosén, A. Comparison of integral equations for the Maxwell transmission problem with general permittivities. *Adv. Comput. Math. 47*, 5 (2021), Paper No. 76, 32.

[18] Helsing, J., and Rosén, A. Dirac integral equations for dielectric and plasmonic scattering. *Integral Equations Operator Theory 93*, 5 (2021), Paper No. 48, 41.

[19] Hiptmair, R. Boundary element methods for eddy current computation. In *Boundary element analysis*, vol. 29 of *Lect. Notes Appl. Comput. Mech.* Springer, Berlin, 2007, pp. 213–248.

[20] Huang, J., Cao, Y., Raimundo, X., Cheema, A., and Salous, S. Rain statistics investigation and rain attenuation modeling for millimeter wave short-range fixed links. *IEEE Access 7* (2019), 156110–156120.

[21] Jackson, J. D. *Classical electrodynamics*, third ed. John Wiley & Sons, Inc., New York-London-Sydney, 1998.

[22] Karlsson, A., and Kristensson, G. Electromagnetic scattering from subterranean obstacles in a stratified ground. *Radio Science 18(03)* (1983), 345–356.

[23] Kress, R. On an exterior boundary value problem for the time-harmonic Maxwell equations with boundary conditions for the normal components of the electric and magnetic field. *Math. Methods Appl. Sci. 8*, 1 (1986), 77–92.

[24] Mikhlin, S. G. *Integral equations and their applications to certain problems in mechanics, mathematical physics and technology*, revised ed. A Pergamon Press Book. The Macmillan Company, New York, 1964. Translated from the Russian by A. H. Armstrong.

[25] Pauly, D., and Picard, R. A note on the justification of the eddy current model in electrodynamics. *Math. Methods Appl. Sci. 40*, 18 (2017), 7104–7109.

[26] ROSÉN, A. *Geometric multivector analysis.* Birkhäuser Advanced Texts: Basler Lehrbücher. [Birkhäuser Advanced Texts: Basel Textbooks]. Birkhäuser/Springer, Cham, [2019] ©2019. From Grassmann to Dirac.

[27] RUCKER, W., HOSCHEK, R., AND RICHTER, K. Various bem formulations for calculating eddy currents in terms of field variables. *IEEE Transactions on Magnetics 31*, 3 (1995), 1336–1341.

[28] SHAMSAN, Z. A. Dust storm and diffraction modelling for 5G spectrum wireless fixed links in arid regions. *IEEE Access 7* (2019), 162828–162840.

[29] SHNEIDER, M. N., AND MILES, R. B. Microwave diagnostics of small plasma objects. *Journal of Applied physics 98*, 3 (2005).

[30] SIFUENTES, J., GIMBUTAS, Z., AND GREENGARD, L. Randomized methods for rank-deficient linear systems. *Electron. Trans. Numer. Anal. 44* (2015), 177–188.

[31] VALDÉS, F., ANDRIULLI, F. P., BAGCI, H., AND MICHIELSSEN, E. A Calderón-preconditioned single source combined field integral equation for analyzing scattering from homogeneous penetrable objects. *IEEE Trans. Antennas and Propagation 59*, 6, part 2 (2011), 2315–2328.

[32] YOUNG, P., HAO, S., AND MARTINSSON, P. G. A high-order Nyström discretization scheme for boundary integral equations defined on rotationally symmetric surfaces. *J. Comput. Phys. 231*, 11 (2012), 4142–4159.

[33] ZHU, Z., SONG, B., AND WHITE, J. Algorithms in fastimp: a fast and wide-band impedance extraction program for complicated 3-d geometries. *IEEE Transactions on Computer-Aided Design of Integrated Circuits and Systems 24*, 7 (2005), 981–998.